Int. J. Nonlinear Anal. Appl. In Press, 1–29
ISSN: 2008-6822 (electronic)
http://dx.doi.org/10.22075/ijnaa.2025.37143.5420

Modeling the impact of climate change transmission dynamics in Ethiopia

Abraham Girma Lemma[a,*], Bewketu Teshale Bekele[b], Getachew Teshome Tilahun[c]

[a]Department of Mathematics, Bule Hora University, Bule Hore, Ethiopia
[b]Department of Mathematics, Debremarkos University, Debremarkos, Ethiopia
[c]Department of Mathematics, Haramaya University, Harar, Ethiopia

(Communicated by Haydar Akca)

Abstract

Dengue is a serious disease that poses a threat to humans in tropical and subtropical regions globally. The disease is transmitted by Aedes type of female mosquitoes, which are highly sensitive to climate change, as changing climate conditions facilitate both pathogen growth and mosquito reproduction. In this study, we investigated how climate variables, especially temperature and rainfall, affect dengue transmission to model disease outbreaks. We developed a deterministic model incorporating temperature and rainfall as climate-related factors, to predict how climate change affects dengue transmission dynamics, thereby supporting public health strategies. We also derived the basic reproduction number (R_0), along with stability analysis to determine the system's steady-state behavior. The disease-free equilibrium is stable when R_0 is less than one, while an endemic equilibrium indicates the disease persists in the community. Moreover, we examined how sensitive parameters influence R_0. Unmanaged temperature and rainfall can significantly intensify dengue outbreaks. Human activities that increase carbon dioxide levels may raise temperatures, further exacerbating the situation. Our simulations show that temperatures between 20 and 30.8 degrees Celsius and rainfall below 50mm can cause an uptick in the mosquito population, which ultimately leads to dengue cases and deaths. The model is also validated using real data and found to be the best fit. Overall, the climate changes at these thresholds can result in a larger mosquito population, increasing the spread of dengue. This model offers a numerical basis for predicting how climate variables impact dengue transmission dynamics.

Keywords: Dengue transmission, Impact of Climate, Aedes aegypti, Vector-born disease
2020 MSC: 92D30

1 Introduction

Dengue fever is a significant public health concern caused by a virus transmitted to humans through the bites of infected female Aedes mosquitoes, primarily Aedes aegypti and Aedes albopictus. These mosquitoes can carry one of four dengue virus serotypes, which complicates the disease's epidemiology and control efforts [28]. In Ethiopia, from January 1, 2023, to January 1, 2025, over 29,494 cases of dengue and 21 deaths have been reported. Of these cases, the

*Corresponding author
Email addresses: abrgirma12@gmail.com (Abraham Girma Lemma), bewketu.bekele@gmail.com (Bewketu Teshale Bekele), gmgech@gmail.com (Getachew Teshome Tilahun)

Received: March 2025 *Accepted:* November 2025

majority 29,028 were documented in the Afar, Dire Dawa, and Somali regions [7]. This growing burden underscores the urgency of our work in Ethiopia, particularly in regions at heightened risk for dengue transmission.

The spread of dengue is influenced by climatic factors like temperature and rainfall, which affect mosquito breeding and life cycles. For example, a temperature increase of 0.5°C can lead to extreme rise in the mosquito population, and higher temperatures accelerate mosquito breeding and pathogen growth [22]. Rainfall also boosts Aedes aegypti populations and hatching rates, particularly when temperatures are elevated [18].

To analyze these factors affecting dengue spread, mathematical modeling is essential for forecasting outbreaks and understanding disease dynamics. Various studies have employed models based on the SIR framework, with early research focusing on the stability of dengue spread. For instance, in historical background of modeling of dengue, [8] were the earliest who studied the global stability and endemic equilibrium of dengue to explore stability at equilibria without considering climate factor. Recently, such notions have been advanced by incorporating various deterministic factor, such as impact of climate variability.

Most of the studies on impact of climate change on dengue spread were focused on theoretical analysis and representative concentration pathway (RCP) approach [13, 14]. Though RCPs are a valuable devices for climate modeling and discussing of associated phenomenon, some gaps such as it focuses on atmospheric concentration of Green House Gas(GHG) instead of emission pathways which can make it tough to relate them to emission reduction; it may not adequately capture local or regional climate dynamics, as it emphasizes on global scale; it do not directly correspond to specific climate policies or consent, that making harder to assess the impact of particular mitigation effort. Similarly, [26] employed shared socioeconomic pathways(SSP) to predict the impact of climate change on dengue transmission. While SSPs are a powerful tools for explaining socioeconomic future and their relation with impacts of climate change on mosquito-born disease, their gaps highlight the need for complementary approach. These include, it does not specify a detailed policy pathways which is difficult to translate into actionable measure, do not account for non-linear change that may happen like a pandemic disease, insufficient granularity for understanding local socioeconomic and climate impact to make decision. However, much of the literature has emphasized theoretical analyses and has not properly addressed local climate dynamics or practical policy implications.

Despite numerous studies on dengue modeling, the existing methods fail to comprehensively account the relationship between dengue transmission and climate change in detail. To bridge this gap, we developed an enhanced model that includes climate variables such as temperature and rainfall alongside human activities contributing to greenhouse gas emissions. To assess this impact, we selected Dire Dawa, Afar, and Somali regions in Ethiopia and have made analysis on monthly mean temperature and rainfall of each region. The model is validated using case data from these regions. Its goal is to predict the impact of climate change on dengue transmission, ultimately informing public health strategies.

The paper is structured as follows: Section (2) outlines the model's description and assumptions; Section (3) presents the analysis of the model; Section (4) discusses climate-related entomological parameters and seasonal variation; Section (5) deals model validation; Section (6) covers the numerical solutions and simulations. Lastly, results with discussion and conclusion are given in section (7) and (8) respectively.

2 Model Description and Formulation

The model incorporates both human and mosquito populations. The human population is divided into susceptible (S_h), exposed (E_h), infected (I_h), and recovered (R_h) categories, while the mosquito population consists of susceptible (S_m), exposed (E_m), and infected (I_m) classes. Due to the short lifespan of mosquitoes, the recovery state is not included in their population structure.

In the human population, susceptible individuals (S_h) can contract dengue when bitten by an infected Aedes mosquito (I_m), moving into the exposed class (E_h). After an average latent period of 4-10 days (approximately 7 days) [28], individuals transition to the infectious class (designated as δE_h). Those who develop immunity and survive dengue move to the recovered class (ϕI_h), while others may move to the infection (denoted as dI_h).

Similarly, the birth rate of mosquitoes contributes to an increase in the susceptible mosquito population. This growth rate can be described by the logistic expression
$(1 - \frac{N_m}{K})\theta(T, R_a)N_m$, which accounts for the maturation of immature mosquitoes into adults (S_m). Once they reach the susceptible stage, they can become exposed if they bite an infected person (I_h). Exposed mosquitoes then move to the infectious class ($\rho(T)E_m$), and it is assumed they live with the infection for their entire lifespan. The mosquito mortality rate ($\mu_m(T)$) and biting rate ($b(T)$) are both influenced by temperature. Additionally, $\theta(T, R_a)$ represents

the extrinsic growth rate of the mosquito population, which is primarily dependent on factors such as temperature and rainfall.

The proposed model considers rainfall and temperature to analyze their effects on disease transmission. While several studies have examined the impact of temperature on the reproduction, survival, and disease transmission capabilities of Aedes mosquitoes, the mathematical modeling approaches for assessing how temperature and rainfall influence the risk of dengue outbreaks remain under-explored. Consequently, we incorporate these factors as functions of the rate of change over time (t). For temperature dynamics, we consider carbon dioxide emissions released into the environment due to human related activities and natural events. In this context, G_n denotes the rate of carbon dioxide emitted from natural sources (such as volcanic eruptions, wildfires, and decomposition), while G_h represents emissions from anthropogenic activities (such as deforestation, industrialization, and transportation). Additionally, γ indicates the the rate of depletion/removal/ of carbon dioxide due to natural activities such as plant photosynthesis, and Ocean absorption r is the rate of temperature rise, and η is the natural rate of temperature depletion.

Furthermore, rainfall affects the rate of change in the mosquito carrying capacity ($K(t)$), which varies with heavy rainfall events and is constrained by a maximum mosquito-host ratio ($K(t) < M_{max}$). Incorporating this state enable us the model handles inappropriate outbreak of disease report. In this framework, R_a represents mean rainfall, b_n indicates the rate of new mosquito breeding sites, b_d represents the rate of breeding sites destroyed by human activity, D_h reflects the likely displaced human population due to high rainfall, and $(1 - D_h)$ indicates the local infection probability considering the impact of displaced human, which represents the portion of population vulnerable to local dengue infection. Hence, the product $b\alpha(1 - D_h)$ is effective transmission rate of dengue, where b is a biting rate and α stands for transmission probability.

The assumptions of the model include all parameters being non-negative, the natural death rate being consistent across all population segments, the focus on the Aedes aegypti mosquito species. Additionally, we assume that dengue virus transmission occurs solely through direct contact between humans and female Aedes mosquitoes.

Based on the above descriptions and assumptions, the model is represented diagrammatically in Figure 1. Later on, system of non-linear differential equations is formulated to represent dengue transmission and analyze it's properties. Moreover, the values and source of parameters are given in Table 2. Here is the diagrammatic scheme of the mathematical model of dengue transmission dynamics under the influence of climate change:

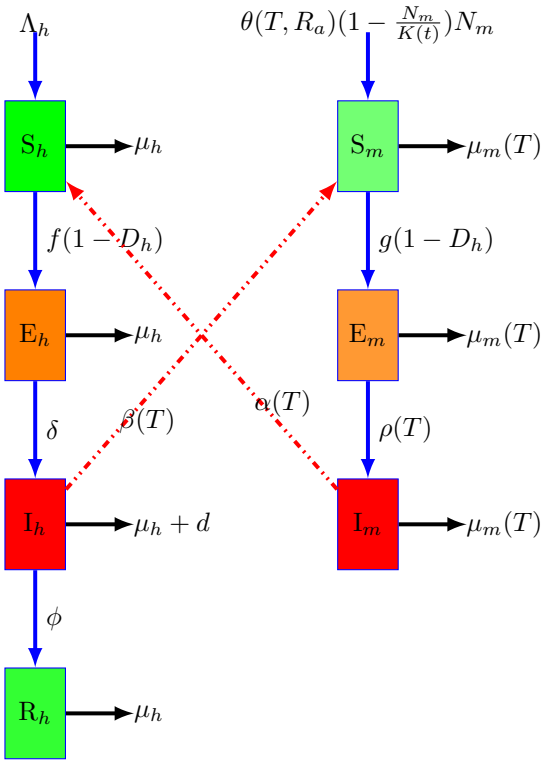

Figure 1: Diagrammatical representation of dengue transmission dynamics and impact of climate on aedes mosquito

Overall, a new system of differential equations deriving the dynamics of rainfall and temperature that adopted to [5, 10, 24], dengue virus transmission model which represented in Figure 1 can be written as

$$\begin{cases} \frac{dS_h(t)}{dt} &= \Lambda_h - f(1-D_h)S_h(t) - \mu_h S_h(t) \\ \frac{dE_h(t)}{dt} &= f(1-D_h)S_h(t) - (\mu_h+\delta)E_h(t) \\ \frac{dI_h(t)}{dt} &= \delta E_h(t) - (d+\phi+\mu_h)I_h(t) \\ \frac{dR_h(t)}{dt} &= \phi I_h(t) - \mu_h R_h(t) \\ \frac{dS_m(t)}{dt} &= \theta(T,R_a)(1-\frac{N_m}{K(t)})N_m - (1-D_h(t))gS_m(t) - \mu_m(T)S_m(t) \\ \frac{dE_m(t)}{dt} &= (1-D_h(t))gS_m(t) - (\mu_m(T)+\rho(T))E_m(t) \\ \frac{dI_m(t)}{dt} &= \rho(T)E_m(t) - \mu_m(T)I_m(t) \\ \frac{dC(t)}{dt} &= G_n + G_h(\Lambda_h - \mu_h N_h) - \gamma\, C(t) \\ \frac{dT(t)}{dt} &= r(C(t)-C_0) - \eta(T(t)-T_0) \\ \frac{dK(t)}{dt} &= b_n N_h R_a(t) - b_d(1-D_h(t))K(t) \end{cases} \tag{2.1}$$

where $f = \frac{\alpha(T)b(T)I_m(t)}{N_h}$ is dengue force of infection from infected Aedes female mosquito to susceptible human S_h and $g = \frac{\beta(T)b(T)I_h(t)}{N_h}$ is transmission force from infected human to susceptible mosquito with initial conditions of the system (2.1) of state variables, $S_h(0) > 0, E_h(0) \geq 0, I_h(0) \geq 0, R_h(0) \geq 0, S_m(0) > 0, E_m(0) \geq 0, I_m(0) \geq 0, T(0) \geq 0, C(0) \geq 0, K(0) \geq 0$.

3 Model Analysis

In this section, the fundamental model analysis such as invariant region of the solution, positivity and the basic reproduction number of model (2.1) are discussed.

3.1 Invariant region

To determine a region in which the solution of system (2.1) is bounded, one can see the following theorem.

Theorem 3.1. The solutions of system of model (2.1) are contained in the feasible region Ω where
$\Omega = \Omega_h \times \Omega_m \times \Omega_c$ such that
$\Omega_h = \{(S_h(t), E_h(t), I_h(t), R_h(t)) \in R_+^4 : S_h(t) + E_h(t) + I_h(t) + R_h(t) \leq \frac{\Lambda_h}{\mu_h}\}$,
$\Omega_m = \{(S_m(t), E_m(t), I_m(t)) \in R_+^3 : S_m(t) + E_m(t) + I_m(t) \leq \frac{(\theta-\mu_m)K}{\theta}\}$ and
$\Omega_c = \{(T, C, K) : T_0 < T < T_{max}, C_0 < C < C_{max}, K_0 < K(t) < M_{max}\}$ is positively bounded.

Proof . From total number of human population we have,

$$N_h(t) = S_h(t) + E_h(t) + I_h(t) + R_h(t). \tag{3.1}$$

Then, differentiating equation (3.1) with respect to time we obtain

$$\frac{dN_h(t)}{dt} = \frac{dS_h(t)}{dt} + \frac{dE_h(t)}{dt} + \frac{dI_h(t)}{dt} + \frac{dR_h(t)}{dt}. \tag{3.2}$$

Substituting (2.1) into (3.2) we get,

$$\frac{dN_h(t)}{dt} = \Lambda_h - \mu(S_h(t) + E_h(t) + I_h(t) + R_h(t)) - dI_h(t). \tag{3.3}$$

Substituting equation (3.7) into (3.3) we get,

$$\frac{dN_h(t)}{dt} = \Lambda_h - \mu_h N_h(t) - dI_h(t). \tag{3.4}$$

In the absence of mortality due to dengue fever disease ($d = 0$), so that equation (3.4) or Without losing the general rule of inequality, Eq. (3.4) become,

$$\frac{dN_h(t)}{dt} \leq \Lambda_h - \mu_h N_h(t). \tag{3.5}$$

Solving the inequality of (3.5) by applying integral and applying the initial condition $N_h(0)$ we get, $N_h(t) \leq \frac{\Lambda_h}{\mu_h} + \frac{N_h(0)}{\mu_h} e^{-t}$, as $t \to \infty$, $N_h(t) \leq \frac{\Lambda_h}{\mu_h}$.

Thus, all feasible solutions of human population of the system (2.1) are contained in the domain Ω_h.

$$\Omega_h = \left\{ (S_h(t), E_h(t), I_h(t), R_h(t)) \in R_+^4 : 0 < N_h(t) \leq \frac{\Lambda_h}{\mu_h} \right\}. \tag{3.6}$$

In the same fashion, let the number of total mosquito is given by:

$$N_m(t) = S_m(t) + E_m(t) + I_m(t). \tag{3.7}$$

Then, differentiating equation of (3.7) with respect to time we obtain:

$$\frac{dN_m(t)}{dt} = \frac{dS_m(t)}{dt} + \frac{dE_m(t)}{dt} + \frac{dI_m(t)}{dt}. \tag{3.8}$$

Substituting (2.1) into (3.8) we get,

$$\frac{dN_m(t)}{dt} = \theta(1 - \frac{N_m(t)}{K})N_m(t) - \mu_m(S_m(t) + E_m(t) + I_m(t). \tag{3.9}$$

Replacing equation of (3.7) into (3.9) we obtain,

$$\frac{dN_m(t)}{dt} = \theta(1 - \frac{N_m(t)}{K})N_m(t) - \mu_m N_m(t). \tag{3.10}$$

Without losing the general rule of inequality, equation (3.10) become,

$$\frac{dN_m(t)}{dt} \leq \theta(1 - \frac{N_m(t)}{K})N_m(t) - \mu_m N_m(t). \tag{3.11}$$

Solving the inequality of (3.11) by applying integral and simplifying further we get, $N_m(t) \leq \frac{(\theta-\mu_m)Ke^t}{\theta e^t + K}$, and as $t \to \infty$, $N_m(t) \leq \frac{(\theta-\mu_m)K}{\theta}$, assuming $\theta - \mu_m > 0$.
Thus, the feasible solution set of mosquito dynamics remain in the region Ω_m.

$$\Omega_m = \left\{ (S_m, E_m, I_m) \in R_+^3 : 0 < N_m(t) \leq \frac{(\theta - \mu_m)K}{\theta} \right\}. \tag{3.12}$$

Similarly, $T_0 < T < T_{max}, C_0 < C < C_{max}$, $K_0 < K(t) < M_{max}$, where M_{max} is maximum number of mosquito to host ratio and $T_{max} = \frac{rG_h\Lambda_h}{\eta\,\gamma} + T_0$, $M_{max} = \frac{N_{m,max}}{N_h}$, $C_{max} = C_0 + \frac{G_h\Lambda_h}{\gamma}$ So that,

$$\Omega_c = \{(T, C, K) : T_0 < T < T_{max},\ C_0 < C < C_{max},\ K_0 < K(t) < M_{max}\} \tag{3.13}$$

Combining equation (3.6), (3.12), and (3.13) we get,

$$\begin{aligned} \Omega &= \Omega_m \times \Omega_h \times \Omega_c \\ &= \{(S_h(t), E_h(t), I_h(t), R_h(t), S_m(t), E_m(t), I_m(t), T(t), C(t), K(t)) \in R_+^{10} \\ &: 0 < N_h(t) \leq \frac{\Lambda_h}{\mu_h}; 0 < N_m(t) \leq \frac{(\theta - \mu_m)K}{\theta}\}. \end{aligned} \tag{3.14}$$

Therefore, model (2.1) is mathematically feasible in the domain (3.14) and so that epidemiologically meaningful. Hence, it is possible to investigate system (2.1) further on the set of region (3.14).□

3.2 Positivity of the Solutions

We assumed that the initial condition of system (2.1) is nonnegative, and now we want to show that the future solution of the model is also positive. To ensure this, we considered the following theorem.

Theorem 3.2. Let $\Omega = \{(S_h, E_h, I_h, R_h, S_m, E_m, I_m, T, C, K) \in \mathbb{R}^{10}_+ : S_h(0) > 0, E_h(0) \geq 0, I_h(0) \geq 0, R_h(0) \geq 0, S_m(0) > 0, E_m(0) \geq 0, I_m(0) \geq 0, T(0) \geq 0, C(0) \geq 0, K(0) \geq 0\}$, then the solutions $\{S_h(t), E_h(t), I_h(t), R_h(t), S_m(t), E_m(t), I_m$ R^{10}_+ are positive for $t > 0$.

Proof . From the system of differential Eq. given in (2.1), taking the first equation become,

$$\frac{dS_h}{dt} = \Lambda_h - f(1 - D_h)S_h(t) - \mu_h S_h(t). \tag{3.15}$$

Then without loosing the general fact of inequality, Eq. (3.15) become

$$\frac{dS_h}{dt} \leq \Lambda_h - \mu_h S_h(t). \tag{3.16}$$

Applying integral and rearranging we get,

$$S_h(t) \leq \frac{\Lambda_h}{\mu_h} - \frac{S_0 e^{-\mu_h t}}{\mu_h}. \tag{3.17}$$

But as $t \to \infty$, $S_0 e^{-\mu_h t} \to 0$. Thus,

$$0 < S_h(t) \leq \frac{\Lambda_h}{\mu_h}. \tag{3.18}$$

From the second equation of system (2.1) we have,
$\frac{dE_h}{dt} = f(1 - D_h)S_h(t) - \delta E_h(t) - \mu_h)E_h(t)$.

Employing inequality become,
$\frac{dE_h}{dt} \geq -\mu_h E_h(t)$.

Integrating this inequality become,
$E_h(t) \geq E_0 e^{-\mu_h t}$. But as $t \to \infty$, $E_0 e^{-\mu_h t} \to 0$. Hence,

$$E_h(t) \geq 0. \tag{3.19}$$

From the third equation of system (2.1) we get,
$\frac{dI_h}{dt} = \delta E_h(t) - (\phi + \mu_h + d)I_h(t)$.

$\frac{dI_h}{dt} \geq -\mu_h I_h(t)$.

$I_h(t) \geq I_0 e^{-\mu_h t}$. But as $t \to \infty$, $I_0 e^{-\mu_h t} \to 0$.

$$I_h(t) \geq 0. \tag{3.20}$$

Similarly, the fourth, fifth, sixth,... tenth equations of system(2.1) become,

$$R_h(t) \geq 0,\ 0 < S_m(t) \leq \frac{K(\theta - \mu_m)}{\theta},\ E_m(t) \geq 0,\ I_m(t) \geq 0,\ T(t) \geq 0,\ C(t) \geq 0,\ K(t) \geq 0. \tag{3.21}$$

Therefore, all solutions of the model are non-negative for $t > 0$.□

3.3 Disease Free Equilibrium

The model given by system (2.1) has a critical point in the absence of dengue disease, which mean $E_h = I_h = E_m = I_m = 0$. Hence, the disease-free equilibrium points ($DFEP$) is obtained by setting the right hand side of each equation of system (2.1) equal to zero, in addition to absence of infective class. Then one can solve for each state in the system. Therefore, the disease free equilibrium point is given by:

$$DFEP = \{\frac{\Lambda_h}{\mu_h}, 0, 0, 0, \frac{K_0(\theta - \mu_m)}{\theta}, 0, 0, T_0, C_0, K_0\}. \tag{3.22}$$

3.4 Basic reproduction number

In this section, we discuss the threshold parameter that governs the spread of a disease which is called *the basic reproduction number(denoted as R_0).* To compute it, one can identify infected states from uninfected class in the system. To proceed, let $\mathcal{F}_k$ be the rate of emergence of new infections in k states and $\mathcal{V}_k = \mathcal{V}_k^- - \mathcal{V}_k^+$ be the difference between the rate of transfer of individual in state k. The function is assumed as continuously differentiable in each variable. The disease transmission model consists of nonnegative initial conditions together with the following system of equations, where x_0 be disease free equilibrium point.

$\frac{dx}{dt} = f_k(x) = \mathcal{F}_k(x) - \mathcal{V}_k(x),\ k = 1, 2, ..., n.$

$$\mathcal{F} = \left[\frac{\partial f_k(x)}{\partial x_i}.\right] \ and\ \mathcal{V} = \left[\frac{\partial v_k(x)}{\partial x_i}.\right] \tag{3.23}$$

where $k \geq 1, i \leq j, j$ is size of matrix or number of infected class and providing $\mathcal{F}$ is nonnegative and $\mathcal{V}$ non-singular M-matrix in which both are $j \times j$ matrix. So that R_0 is the spectral radius of the next generation matrix(i.e $p(\mathcal{F}\mathcal{V}^{-1})$).

In the process of computing R_0 for the system of (2.1), we start with uninfected classes such as S_h, S_m, R_h and then followed by infected; E_h, E_m, I_h, I_m. Rewriting the system of (2.1) we get,

$$\begin{cases} \frac{dS_h}{dt} = \Lambda_h - \frac{b(1-D_h)\alpha I_m(t)S_h(t)}{N_h} - \mu_h S_h(t) \\ \frac{dR_h}{dt} = \phi I_h(t) - \mu_h R_h(t) \\ \frac{dS_m}{dt} = \theta(1 - \frac{N_m}{K})N_m - \frac{(1-D_h)b\beta I_h(t)S_m(t)}{N_h} - \mu_m S_m(t) \end{cases} \tag{3.24}$$

$$\begin{cases} \frac{dE_h}{dt} = \frac{b(1-D_h)\alpha I_m(t)S_h(t)}{N_h} - (\mu_h + \delta)E_h(t) \\ \frac{dI_h}{dt} = \delta E_h(t) - (d + \phi + \mu_h)I_h(t) \\ \frac{dE_m}{dt} = \frac{(1-D_h)b\beta I_h(t)S_m(t)}{N_h} - (\mu_m + \rho)E_m(t) \\ \frac{dI_m}{dt} = \rho E_m(t) - \mu_m I_m(t) \end{cases} \tag{3.25}$$

Now, from equation of (3.25), we show the rate of emergence of newly infected that inter into E_h and E_m states by the help of next generation matrix as follow:

The new infection terms are:

- For E_h: infections coming from contact between susceptible humans and infectious mosquitoes (I_m)
- For E_m: infections coming from contact between susceptible mosquitoes and infectious humans (I_h)

To construct $\mathcal{F}$ and $\mathcal{V}$ at DFE,

$$\begin{aligned} S_h &\approx N_h \quad \text{(initial susceptible human population)} \\ S_m &\approx N_m \quad \text{(initial susceptible mosquito population)} \\ \text{and} \quad &\text{all infected classes are zero.} \end{aligned}$$

F-*vector*:

$\mathcal{F} = \begin{bmatrix} \text{new infections into } E_h \\ \text{new infections into } I_h \\ \text{new infections into } E_m \\ \text{new infections into } I_m \end{bmatrix}$ Since new infections only enter E_h and E_m:

$$\mathcal{F} = \begin{bmatrix} b\alpha(1-D_h)\frac{I_m}{N_h} \times S_h \\ 0 \\ (1-D_h)b\beta\frac{I_h}{N_h} \times S_m \\ 0 \end{bmatrix}$$

Evaluating at DFE ($S_h = N_h = \frac{\Lambda_h}{\mu_h}$, $S_m = N_m = \frac{K_0(\theta-\mu_m)}{\theta}$):

$$\mathcal{F} = \begin{bmatrix} b\alpha(1-D_h)I_m \\ 0 \\ b\beta(1-D_h)\mu_h\frac{K_0(\theta-\mu_m)}{\Lambda_h\theta}I_h \\ 0 \end{bmatrix} \tag{3.26}$$

V-*vector*:

$$\mathcal{V} = \begin{bmatrix} (\mu_h+\delta)E_h \\ (\phi+\mu_h+d)I_h - \delta E_h \\ (\mu_m+\rho)E_m \\ \mu_m I_m - \rho E_m \end{bmatrix} \tag{3.27}$$

Equation (3.27) represents net transfer (outflows minus inflows), excluding new infections.

Computing the Jacobians of $\mathcal{F}$ and $\mathcal{V}$ with respect to $\mathbf{x} = (E_h, I_h, E_m, I_m)$ at DFE((3.22)) we get,

$$\mathcal{F} = \begin{pmatrix} 0 & 0 & 0 & b(1-D_h)\alpha \\ 0 & 0 & 0 & 0 \\ 0 & \frac{(1-D_h)b\beta(\theta-\mu_m)K_0\mu_h}{\theta\Lambda_h} & 0 & 0 \\ 0 & 0 & 0 & 0 \end{pmatrix}. \tag{3.28}$$

Similarly, evaluating the Jacobean matrix of equation (3.27) of the transfer of all individual in stacks by all other means at (3.22) we get,

$$\mathcal{V} = \begin{pmatrix} (\mu_h+\delta) & 0 & 0 & 0 \\ -\delta & (\phi+\mu_h+d) & 0 & 0 \\ 0 & 0 & \mu_m+\rho & 0 \\ 0 & 0 & -\rho & \mu_m \end{pmatrix}. \tag{3.29}$$

The inverse of matrix $\mathcal{V}$ of equation (3.29) become

$$\mathcal{V}^{-1} = \begin{pmatrix} \frac{1}{\delta+\mu_h} & 0 & 0 & 0 \\ \frac{\delta}{(\phi+\mu_h+d)(\mu_h+\delta)} & \frac{1}{\phi+\mu_h+d} & 0 & 0 \\ 0 & 0 & \frac{1}{\rho+\mu_m} & 0 \\ 0 & 0 & \frac{\rho}{\mu_m(\rho+\mu_m)} & \frac{1}{\mu_m} \end{pmatrix}. \tag{3.30}$$

Now, let $G = \mathcal{F}\mathcal{V}^{-1}$ which we denote as the next generation matrix.

$$G = \mathcal{F}\mathcal{V}^{-1} \tag{3.31}$$

$$= \begin{pmatrix} 0 & 0 & 0 & b(1-D_h)\alpha \\ 0 & 0 & 0 & 0 \\ 0 & \frac{(1-D_h)b\beta(\theta-\mu_m)K_0\mu_h}{\theta\Lambda_h} & 0 & 0 \\ 0 & 0 & 0 & 0 \end{pmatrix} \begin{pmatrix} \frac{1}{\delta+\mu_h} & 0 & 0 & 0 \\ \frac{\delta}{(\phi+\mu_h+d)(\mu_h+\delta)} & \frac{1}{\phi+\mu_h+d} & 0 & 0 \\ 0 & 0 & \frac{1}{\rho+\mu_m} & 0 \\ 0 & 0 & \frac{\rho}{\mu_m(\rho+\mu_m)} & \frac{1}{\mu_m} \end{pmatrix}. \tag{3.32}$$

This implies that, the next generation matrix of model (2.1) is:

$$G = \begin{pmatrix} 0 & 0 & \frac{(1-D_h)b\alpha\rho}{\mu_m(\rho+\mu_m)} & \frac{(1-D_h)b\alpha}{\mu_m} \\ 0 & 0 & 0 & 0 \\ \frac{(1-D_h)b\beta\mu_h(\theta-\mu_m)K_0\delta}{\theta\Lambda_h(\mu_h+\delta)(d+\mu_h+\phi)} & \frac{(1-D_h)b\beta\mu_h(\theta-\mu_m)K_0}{\theta\Lambda_h(d+\phi+\mu_h)} & 0 & 0 \\ 0 & 0 & 0 & 0 \end{pmatrix}. \tag{3.33}$$

Now, to get the eigenvalues of matrix of (3.33), we equate determinant of (3.33) with corresponding eigenvalue to zero. To do so,
let $\mathfrak{p}_1 = \frac{(1-D_h)b\alpha\rho}{\mu_m(\rho+\mu_m)}$, $\mathfrak{p}_2 = \frac{(1-D_h)b\alpha}{\mu_m}$, $\mathfrak{p}_3 = \frac{(1-D_h)b\beta\mu_h(\theta-\mu_m)K_0\delta}{\theta\Lambda_h(\mu_h+\delta)(d+\mu_h+\phi)}$ and $\mathfrak{p}_4 = \frac{(1-D_h)b\beta\mu_h(\theta-\mu_m)K_0}{\theta\Lambda_h(d+\phi+\mu_h)}$, then

$$\begin{vmatrix} -\lambda & 0 & \mathfrak{p}_1 & \mathfrak{p}_2 \\ 0 & -\lambda & 0 & 0 \\ \mathfrak{p}_3 & \mathfrak{p}_4 & -\lambda & 0 \\ 0 & 0 & 0 & -\lambda \end{vmatrix} = 0. \tag{3.34}$$

Solving (3.34) and substituting the values of $\mathfrak{p}_i$, where $i = 1, 2, 3, 4$ we get,

$$\lambda_1 = \sqrt{\frac{b^2(1-D_h)^2\alpha\beta\delta\rho\mu_h(\theta-\mu_m)K_0}{\mu_m\theta\Lambda_h(d+\mu_h+\phi)(\delta+\mu_h)(\rho+\mu_m)}}, \quad \lambda_2 = -\sqrt{\frac{b^2(1-D_h)^2\alpha\beta\delta\rho\mu_h(\theta-\mu_m)K_0}{\mu_m\theta\Lambda_h(d+\mu_h+\phi)(\delta+\mu_h)(\rho+\mu_m)}} \text{ and } \lambda_{3,4} = 0.$$

As the dominant eigenvalue of the next generation matrix G represents R_0 = maximum eigenvalue of FV^{-1}, thus

$$R_0 = \sqrt{\frac{b^2(1-D_h)^2\alpha\beta\delta\rho\mu_h(\theta-\mu_m)K_0}{\mu_m\theta\Lambda_h(d+\mu_h+\phi)(\delta+\mu_h)(\rho+\mu_m)}}. \tag{3.35}$$

Simplifying equation (3.35) further and splitting it into R_{0h} and R_{0m} we obtain,

$$\begin{aligned} R_0 =& \sqrt{\frac{b^2(1-D_h)^2\alpha\beta\delta\rho\mu_h(\theta-\mu_m)K_0}{\mu_m\theta\Lambda_h(d+\mu_h+\phi)(\delta+\mu_h)(\rho+\mu_m)}} \\ =& \sqrt{\frac{(1-D_h)b\alpha\delta}{(d+\mu_h+\phi)(\delta+\mu_h)}} \times \sqrt{\frac{(1-D_h)\mu_h b\beta\rho(\theta-\mu_m)K_0}{\mu_m\theta\Lambda_h(\rho+\mu_m)}} \\ =& \sqrt{R_{0h} \times R_{0m}}. \end{aligned} \tag{3.36}$$

Generally, R_{0h} is the average number of humans that one Aedes mosquito can produce infection in the whole susceptible humans during its infectious lifetime. But, R_{0m} is the mean number of Aedes mosquitoes in which one human infects the entirely susceptible mosquito dynamics through their infectious period.

3.5 Local Stability of Disease free Equilibrium

Theorem 3.3. The disease free equilibrium point (3.22) is locally asymptotically stable in the feasible region Ω if $R_0 < 1$ and otherwise unstable.

Proof . To analyze the local stability of the disease-free equilibrium (DFE) for the system (2.1), first we linearize the subsystem of infected part, so that the Jacobian matrix J can be partitioned into blocks for infected (E_h, I_h, E_m, I_m) and uninfected compartments. However, the critical block for stability is the infected subsystem [1, 4] of Jacobian evaluated at DFE:

$$J_{\text{infected}} = \begin{bmatrix} -(\mu_h+\delta) & 0 & 0 & (1-D_h)b\alpha \\ \delta & -(d+\phi+\mu_h) & 0 & 0 \\ 0 & (1-D_h)b\beta\mu_h\frac{K_0(\theta-\mu_m)}{\theta\Lambda_h} & -(\mu_m+\rho) & 0 \\ 0 & 0 & \rho & -\mu_m \end{bmatrix}. \tag{3.37}$$

To determine if all eigenvalues of the Jacobian matrix J_{infected} have negative real parts (ensuring local stability of the DFE when $R_0 < 1$), we analyze the characteristic equation obtained from Eq. (3.37):

$$(\lambda + \mu_h + \delta)(\lambda + d + \phi + \mu_h)(\lambda + \mu_m + \rho)(\lambda + \mu_m) - \frac{(1 - D_h)^2 b^2 \alpha\beta\delta\rho\mu_h K_0(\theta - \mu_m)}{\theta\Lambda_h} = 0 \tag{3.38}$$

Expanding the characteristic equation of (3.38) we get,

$$\begin{aligned} P(\lambda) &= \lambda^4 + [d + \phi + 2\mu_h + \delta + 2\mu_m + \rho]\lambda^3 \\ &+ \left[(d + \phi + 2\mu_h + \delta)(2\mu_m + \rho) + (\mu_h + \delta)(d + \phi + \mu_h) + \mu_m^2 + \mu_m\rho\right]\lambda^2 \\ &+ \left[(d + \phi + 2\mu_h + \delta)(\mu_m^2 + \mu_m\rho) + (\mu_h + \delta)(d + \phi + \mu_h)(2\mu_m + \rho)\right]\lambda \\ &+ (\mu_h + \delta)(d + \phi + \mu_h)(\mu_m^2 + \mu_m\rho) - \frac{(1 - D_h)^2 b^2 \alpha\beta\delta\rho\mu_h K_0(\theta - \mu_m)}{\theta\Lambda_h}. \end{aligned} \tag{3.39}$$

$$\begin{aligned} \text{Let } a_3 &= [d + \phi + 2\mu_h + \delta + 2\mu_m + \rho] \\ , a_2 &= [(d + \phi + 2\mu_h + \delta)(2\mu_m + \rho) + (\mu_h + \delta)(d + \phi + \mu_h) + \mu_m^2 + \mu_m\rho], \\ a_1 &= [(d + \phi + 2\mu_h + \delta)(\mu_m^2 + \mu_m\rho) + (\mu_h + \delta)(d + \phi + \mu_h)(2\mu_m + \rho)] \\ , a_0 &= [(\mu_h + \delta)(d + \phi + \mu_h)(\mu_m^2 + \mu_m\rho)] - \frac{(1 - D_h)^2 b^2 \alpha\beta\delta\rho\mu_h K_0(\theta - \mu_m)}{\theta\Lambda_h} \\ &= [\mu_m(\mu_h + \delta)(d + \phi + \mu_h)(\mu_m + \rho)](1 - R_0) \end{aligned} \tag{3.40}$$

Now, we employ Routh-Hurwitz criterion to analyze as all coefficients are positive, so that all eigenvalues are negative real part. Hence, for a quartic polynomial

$$\lambda^4 + a_3\lambda^3 + a_2\lambda^2 + a_1\lambda + a_0 = 0,$$

we test the Routh-Hurwitz conditions for stability (all roots with negative real parts). However, since all parameters in system (2.1) are non-negative, their sum is also non-negative. Consequently, the coefficients a_3, a_2, a_1 are all positive, as they are sums of model parameters. For $a_0 > 0$, it is necessary that $R_0 < 1$, according to equation (3.40). When $R_0 < 1$, all coefficients of the characteristic polynomial are positive, and the Routh-Hurwitz conditions are satisfied.

By Routh-Hurwitz criterion, all eigenvalues have negative real parts, confirming the local asymptotic stability of the DFE.

Therefore, DFE is locally asymptotically stable when $R_0 < 1$, and otherwise unstable. □

3.6 Existence of Endemic Equilibrium

The endemic equilibrium is a point whereby dengue disease present in the population which is given by, $EE = (S_h^\star, E_h^\star, I_h^\star, R_h^\star, S_m^\star, E_m^\star, I_m^\star, T^\star, C^\star, K^\star)$. This equilibrium is occurs when the disease persists in the community. To obtain it, we equate each of the equations in (2.1) to zero.

Solving for each compartments given by (2.1) we get,

$$
\begin{aligned}
S_h^\star(t) &= \frac{\Lambda_h}{(1-D_h)f^\star+\mu_h},\\
E_h^\star(t) &= \frac{\Lambda_h b}{\delta\,(1-D_h)f^\star+\delta\,\mu_h+(1-D_h)f^\star\mu_h+{\mu_h}^2},\\
I_h^\star(t) &= \frac{\delta\, b\Lambda_h}{d\delta\,(1-D_h)f^\star+L_1^\star+{\mu_h}^2\phi},\\
R_h^\star(t) &= \frac{\delta\,\mu_h\, b\Lambda_h}{\phi\left(d\delta\,(1-D_h)f^\star+L_2^\star+\delta\,{\mu_h}^2+\delta\,\mu_h\,\phi+(1-D_h)f^\star{\mu_h}^2+(1-D_h)f^\star\mu_h\,\phi+{\mu_h}^3+{\mu_h}^2\phi\right)},\\
S_m^\star(t) &= \frac{\theta}{(1-D_h)g^\star+\mu_m}\\
E_m^\star(t) &= \frac{(1-D_h)g^\star\theta}{(1-D_h)g^\star\rho+(1-D_h)g^\star\mu_m+\rho\,\mu_m+{\mu_m}^2},\\
I_m^\star(t) &= \frac{(1-D_h)g^\star\rho\,\theta}{\mu_m((1-D_h)g^\star\rho+(1-D_h)g^\star\mu_m+\rho\,\mu_m+{\mu_m}^2)}.\\
T^\star &= \frac{rG_h\Lambda_h}{\eta\,\gamma}+T_0\\
C^\star &= C_0+\frac{G_h\Lambda_h}{\gamma}\\
K^\star &= \frac{N_{m,max}^\star}{N_h^\star}
\end{aligned}
\tag{3.41}
$$

where $f^\star=\frac{b\alpha I_m^\star}{N_h^\star}$ and $g^\star=\frac{b\beta I_h^\star}{N_h^\star}$ are infection force of dengue, $L_1^\star=d\delta\,\mu_h+d(1-D_h)f^\star\mu_h+d{\mu_h}^2+\delta\,(1-D_h)f^\star\mu_h+\delta\,(1-D_h)f^\star\phi+\delta\,{\mu_h}^2+\delta\,\mu_h\,\phi+(1-D_h)f^\star{\mu_h}^2$
$+(1-D_h)f^\star\mu_h\,\phi+{\mu_h}^3$ and $L_2^\star=d\delta\,\mu_h+d(1-D_h)f^\star\mu_h+d{\mu_h}^2+\delta\,(1-D_h)f^\star\mu_h+\delta\,(1-D_h)f^\star\phi$. Note that L_1 and L_2 represent the expanded values of $I_h^\star$ and $R_h^\star$, respectively, in equation (3.41). From the values obtained in equation (3.41), we observe that the solutions $S_h^\star$, $E_h^\star$, $I_h^\star$, $R_h^\star$, $S_m^\star$, $E_m^\star$, $I_m^\star$, $T^\star$, $C^\star$, and $K^\star$ are positive and unique. The following theorem emphasizes the global stability of the endemic equilibrium.

3.7 The global stability of endemic equilibrium

Theorem 3.4. If $R_0>1$, then there exist a unique positive endemic equilibrium in invariant set $\mathbb{D}_2\subset\Omega$ such that any trajectories starting in $\mathbb{D}_2$ converges to EE as $t\to\infty$, resulting EE is globally asymptotically stable, where Ω is invariant region for system (2.1).

Proof . To prove this theorem, we employed Monotonicity theorem(MT), as it is a powerful theorem that design the ways to show existence or absence of disease via the given equilibria. To proceed, we create a subsystem that directly associate with the disease as:

$$
\begin{cases}
\frac{dE_h}{dt}=\frac{b(1-D_h)\alpha I_m(t)S_h(t)}{N_h}-(\mu_h+\delta)E_h(t)\\
\frac{dI_h}{dt}=\delta E_h(t)-(d+\phi+\mu_h)I_h(t)\\
\frac{dE_m}{dt}=\frac{(1-D_h)b\beta I_h(t)S_m(t)}{N_h}-(\mu_m+\rho)E_m(t)\\
\frac{dI_m}{dt}=\rho E_m(t)-\mu_m I_m(t)
\end{cases}
\tag{3.42}
$$

Formulating Jacobian matrix of equation (3.42) that evaluated at EE we get,

$$
J_{ee}=\begin{pmatrix}B_{11}&0&0&B_{14}\\ \delta&B_{22}&0&0\\ 0&B_{32}&B_{33}&0\\ 0&0&\rho&B_{44}\end{pmatrix},
\tag{3.43}
$$

where $B_{11}=-(\delta+\mu_h)$, $B_{22}=-(\phi+\mu_h)$, $B_{33}=-(\rho+\mu_h)$, $B_{44}=-\mu_m$,
$B_{14}=(1-D_h)\frac{(bS_h^\star\alpha)N_h^\star-bI_m^\star S_h^\star\alpha}{(N_h^\star)^2}$, and $B_{32}=(1-D_h)\frac{(bS_m^\star\beta)N_h^\star-bI_h^\star S_m^\star\beta}{(N_h^\star)^2}$

For the subsystem (3.42) represented with $X'=\frac{\partial G_i}{\partial x_k}$, where $i\neq k$, the monotonicity theorem addresses;

- $\frac{\partial G_{E_h}}{\partial I_m}=(1-D_h)\frac{(bS_h^\star\alpha)N_h^\star-bI_m^\star S_h^\star\alpha}{(N_h^\star)^2}>0$, this implies that, as E_h increase I_m also increase, where $D\in(0,1)$.

- $\frac{\partial G_{I_h}}{\partial E_h} = \delta > 0$, indicates as I_h increase E_h do so.
- $\frac{\partial G_{E_m}}{\partial I_h} = (1 - D_h)\frac{(bS_m^\star\beta)N_h^\star - bI_h^\star S_m^\star\beta}{(N_h^\star)^2} > 0$, which displays the interaction of E_m and I_h.
- Similarly, $\frac{\partial G_{I_m}}{\partial E_m} = \rho > 0$.

Since all entries of off-diagonal are positive, the monotonicity conditions are satisfied.

Now set the invariant region such that, $\mathbb{D}_2 = \{(E_h, I_h, E_m, I_m) \in \mathbb{R}_+^4 : E_h, I_h, E_m, I_m \geq 0\}$. Therefore, for $R_0 > 1$, by monotonicity theorem, there is a unique positive endemic equilibrium such that all trajectories starting in $\mathbb{D}_2$ converges to EE for $t > 0$. Thus, EE is globally asymptotically stable. □

3.8 Bifurcation Analysis

While stability is well-established within the theoretical framework, bifurcation analysis often encounters gaps related to the precise characterization of transition points and the nature of emergent solutions. Specifically, traditional approaches may lack clarity regarding the local versus global bifurcations and the conditions under which qualitative changes in system behavior occur. The Figure in 2 helps fill these gaps by providing a detailed visualization, illustrating how parameter variations lead to the formation, disappearance, or transformation of equilibrium states. This visual representation clarifies the nonlinear interactions near critical thresholds, thereby bridging the gap between abstract theoretical predictions and their practical manifestations. Consequently, it enhances our understanding of the stability landscape and the mechanisms underlying bifurcation phenomena, offering a more comprehensive picture that integrates local dynamical behaviors with overarching system stability considerations.

Moreover, Figure 2 illustrates a critical threshold at $R_0 = 1$, where the system transitions from a disease-free equilibrium (DFE) to an endemic state. For $R_0 < 1$, the DFE remains stable, indicating that the infection cannot sustain itself within the population, as reflected by the stable green line. However, as R_0 surpasses 1, the stability of the DFE is lost, and an endemic equilibrium emerges, shown by the stable red line, with the infected population increasing steadily. This bifurcation point signifies a forward (trans-critical) bifurcation, emphasizing the importance of controlling R_0 below 1 to prevent disease persistence. The diagram underscores how small changes in R_0 around the critical value can lead to significant shifts in disease dynamics, providing valuable insights for public health interventions aimed at disease eradication. This can be illustrated as:

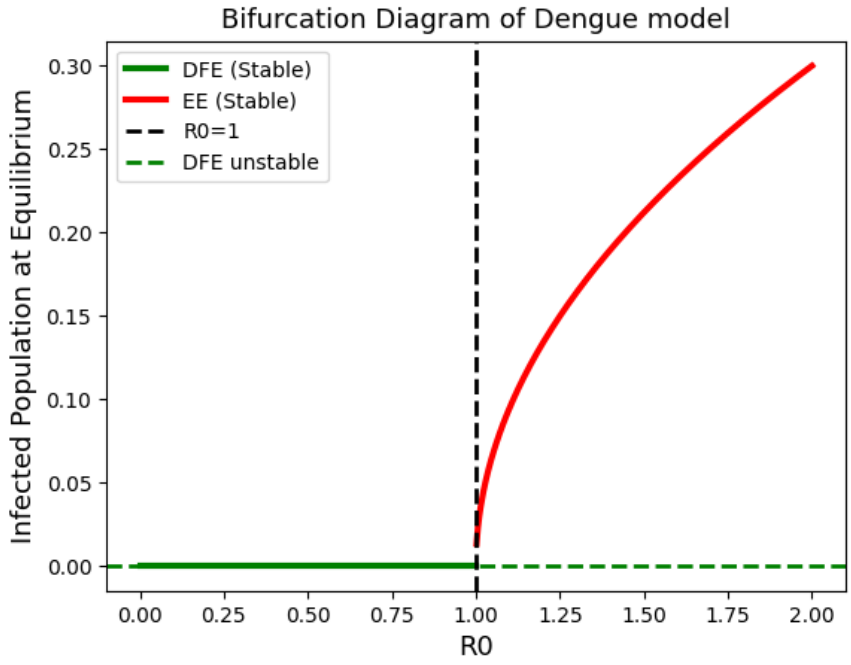

Figure 2: Bifurcation Diagram

3.9 Sensitivity Analysis of Model Parameters

To carryout sensitivity analysis of the model parameters, we employed the following method. This method develop a formula to obtain the sensitivity index of the parameters that critically influence the model dynamics and it is defined as:

$$S_{x_i}^{R_0} = \frac{\partial R_0}{\partial x_i}(\frac{x_i}{R_0}). \tag{3.44}$$

,where x_i represents i^{th} basic parameters, with $i = 1, 2...n$. But from equation (3.35) we have,

$$R_0 = \sqrt{\frac{b^2(1-D_h)^2\alpha\beta\delta\rho\mu_h(\theta-\mu_m)K_0}{\mu_m\theta\Lambda_h(d+\mu_h+\phi)(\delta+\mu_h)(\rho+\mu_m)}}.$$

Computing each parameter by using the formula in Eq. (3.44) and simplifying further we get

$$\begin{aligned}
S_{\alpha}^{R_0} &= \frac{\partial R_0}{\partial \alpha}(\frac{\alpha}{R_0}) \\
S_{\alpha}^{R_0} &= \frac{1}{2}.
\end{aligned}$$

Similarly,

$$\begin{aligned}
&S_{\beta}^{R_0} = S_{K_0}^{R_0} = \frac{1}{2},\ S_{b}^{R_0} = 1,\ S_{\Lambda_h}^{R_0} = -1,\ S_{\rho}^{R_0} = \frac{\mu_m - \rho}{2(\mu_m + \rho)}, \\
&S_{\delta}^{R_0} = \frac{\mu_m - \delta}{2(\mu_m + \delta)},\ S_{\mu_m}^{R_0} = -\frac{2\rho + 3\mu_m}{\rho + \mu_m},\ S_{\phi}^{R_0} = -\frac{\phi}{d + \phi + \mu_h}, \\
&S_{\mu_h}^{R_0} = \frac{(\mu_h + \delta)(d + \mu_h + \phi) - 2\mu_h(2\mu_h + \delta + d + \phi)}{2(\delta + \mu_h)(d + \mu_h + \phi)}, \\
&S_{\theta}^{R_0} = \frac{\theta - 2\mu_m}{2(\mu_m - \theta)},\ S_{d}^{R_0} = -\frac{d}{(d + \phi + \mu_h)}.
\end{aligned} \tag{3.45}$$

The analysis of parameters α, β, and K_0 reveals that they each contribute 50% to the increase of dengue outbreaks. Parameters b is identified as the most sensitive, significantly influencing disease expansion, while μ_m, d, and ϕ show limited sensitivity in disease transmission. A sensitivity value of -1 for the human recruitment rate (Λ_h) means that a one-unit increase in this rate leads to a one unit decrease in the number of new cases, indicating a strong, linear impact on the model's outcome. Conversely, a sensitivity value of +1 for the mosquito biting rate (b) indicates that a one-unit increase results in an equivalent increase in the number of new cases, reflecting a direct and predictable relationship between biting rate and disease prevalence.

4 Model Analysis with Climate-based Parameters

To analyze climate-based parameters, we adopted on system of equation (2.1), so that climate-based entomological parameters are defined. To do so, the monthly mean temperature and rainfall of three regions in Ethiopia were mentioned. The monthly mean temperature and rainfall averages for Dire Dawa, Afar, and the Somali Region in Ethiopia that defined in table available as Supplementary materials, which we consider for our investigation based on climate data obtained from [6].

4.1 Mosquito Birth Rate

Since the birth rate of mosquitoes is influenced by rainfall and temperature, we employed a sophisticated analytical framework of [21, 19] to examine the birth rate of Aedes mosquitoes along with other climate-related entomological parameters. These parameters include the biting rate, mosquito infectious rate, transmission probabilities, and mosquito mortality rate in the Dire Dawa, Afar, and Somali regions. We utilized the parameter values outlined in Table 2, along with regional temperature and rainfall data. The results of our analyses are summarized for each formula used in our study.

The life cycle of mosquitoes is highly influenced by climate change, particularly temperature and rainfall [17, 15]. Therefore, the following formulas address how climate change influence mosquito population dynamics and analysis

demonstrate the potential impact of temperature and rainfall on the mosquito's birth rate and how these factors affect their life cycle.

$$\theta(T, R_a) = \frac{\pi_e H_s(T, R_a) S_l(T, R_a) S_p(R)_a}{\tau_e + \tau_l m(T) + \tau_p}. \tag{4.1}$$

where π_e represents the number of eggs laid per female *Aedes* mosquito. The functions $H_s(T, R_a)$, $S_l(T, R_a)$, and $S_p(R_a)$ denote the survival probabilities of eggs, larvae, and pupae, respectively. Additionally, τ_e, $\tau_l m(T)$, and τ_p represent the average durations of the egg, larval, and pupal stages. Here, T and R_a stand for the mean temperature and rainfall, respectively.

Now, let's highlight the existing literature on the average developmental durations for the larval stage, as used by [19] and [15]:

$$\begin{aligned} \tau_l(T) &= \frac{1}{0.0554T - 0.06737} \\ &\quad \text{which is true if } 0.0554T - 0.06737 > 0 \\ \implies T &> \frac{0.06737}{0.0554} \approx 1.216^o C \end{aligned} \tag{4.2}$$

In reality, Aedes mosquito's larva did not develop at this temperature [17]. Additionally, evaluating the regional optimal mean temperature we obtained: Dire Dawa: $\tau_l(28.2^oC) = 0.067$, Afar: $\tau_l(28.6^oC) = 0.066$ Somali: $\tau_l(27.5^oC) = 0.069$. In reality, Aedes aegypti larvae generally take about 7 to 10 days to develop from hatch to pupation at optimal temperatures (26^oC to 30^oC) [29, 2]. Thus, we leave the formula (4.2) and employed the other formula that align with the reality, so that the average developmental duration $\tau_l m(T)$ in days can be estimated using the formula which is adopted to [3] and match with the fitted one:

$$\tau_l m(T) = \frac{K}{T - T_{min}} \tag{4.3}$$

where $\tau_l m(T)$ be development time of larva in days as a function of T, T = ambient temperature in ^{o}C, T_{min} = lower developmental threshold temperature in ^{o}C, which is often estimated around 10^oC, and K = degree-days required for development (species-specific constant) which is for Aedes aegypti, values around 100 -150 degree-days. Hence, we used the average of degree-days which is 125.

Determining th average development duration of larva for each region we get: Dire Dawa: $\tau_l(28.2^oC) = 6.87$ days, Afar: $\tau_l(28.6^oC) = 6.72$ days, Somali: $\tau_l(27.5^oC) = 7.14$ days. These values indicate that larvae in Dire Dawa and Afar develop slightly faster than those in Somali. The differences may suggest variations in environmental conditions or resource availability that could affect growth rates.

$$S_l(T, R_a) = (e^{0.06737 - 0.0554T}) \frac{4 S_{lmax}}{R_{fl}^2} R_a (R_{fl} - R_a), \tag{4.4}$$

where R_{fl} is the rainfall which can flush out the larva, S_{lmax} maximum survival probability of larva, R_a stands for mean rainfall in the region. Summary of Survival Probabilities of larva in each region:

Dire Dawa: $S_l \approx 0.0334$, Afar:$S_l \approx 0.04702$, Somali: $S_l \approx 0.05767$. From this analysis, we can conclude that the survival probability of larvae is highest in the Somali region, followed by Afar, and is lowest in Dire Dawa. The probability of survival rate of pupa is given as

$$S_p(R_a) = \frac{4 S_{pmax}}{R_{fp}^2} R_a (R_{fp} - R_a), \tag{4.5}$$

where R_{fp} is the rainfall which can flush out the pupa, S_{pmax} maximum survival probability of pupa, R_a stands for mean rainfall in the region. This formula indicates that the survival probability depends on both R_a and R_{f_p} through a quadratic relationship in terms of R_a.

Dire Dawa: $S_p \approx 0.329$, Afar: $S_p \approx 0.473$, and Somali:$S_p \approx 0.549$.

From this analysis, we can conclude that the survival probability of pupae is highest in the Somali region, followed by Afar, and is lowest in Dire Dawa.

4.2 Mosquito hatching success

Aedes mosquito hatching succuss depend on both temperature and rainfall. Hence, the formula is adopted to [23, 19] and given as

$$H_s(T, R_a) = \pi_1(1 - e^{\pi_2(T-40)})\frac{4H_{emax}}{R_{fe}^2}R_a(R_{fe} - R_a), \tag{4.6}$$

where R_{fe} is the rainfall which can flush out the pupa, H_{emax} maximum survival probability of pupa, R_a stands for mean rainfall in the region whose values are given in Table 2. To implement this formula with climate data from three regions we obtain the following results.

The hatching success of each region is summarized as follows:

Dire Dawa: $H_s \approx 0.607$, Afar: $H_s \approx 0.0877$, Somali:$H_s \approx 0.1297$

From this analysis, we conclude the success of the hatching rate is highest in Dire Dawa, followed by Somali, and is lowest in Afar.

Generally, the birth rate of Aedes mosquito generalized below:

Region	$H_s(T, R_a)$	$S_p(R_a)$	$S_l(T, R_a)$	$\theta(T, R_a)$
Diredawa	0.607	0.329	0.0334	0.151
Afar	0.0877	0.473	0.04702	0.045
Somali	0.1297	0.549	0.05767	0.090

Table 1: Summary of Mosquito's birth rate via Climate Change for Different Regions

Table 1 shows that,the highest value of Aedes mosquito birth rate θ is observed in Dire Dawa, followed by Somali, and the lowest is in Afar.

4.3 Adult female mosquito death rate

As life of adult female mosquito determined by temperature, its death rate which was adopted to the quadratic fitting by [17] is given as

$$\mu_m(T) = a_1T^2 + a_2T + a_3, \tag{4.7}$$
$$\text{where T is mean temperature, } a_1 = 0.000193, a_2 = -0.00901, a_3 = 0.123.$$

But to analyze the Aedes mosquito's local death rate, we used the values of temperature described in table available as Supplementary materials so that the death rate results of each region is:

$$\text{Dire Dawa: } \mu_m(28.2) \approx 0.022, \text{ Afar: } \mu_m(28.6) \approx 0.023, \text{ Somali: } \mu_m(27.5) \approx 0.021.$$

From this computations, the death rates of mosquitoes vary across the three regions, with Afar exhibiting the highest death rate at approximately 0.023 per a day, followed closely by Dire Dawa at 0.022 per a day. Somali records the lowest death rate at 0.021 per a day. This indicates that, on average, the lifespan of Aedes mosquito in Dire Dawa, Afar, and Somali accounts 45.45, 43.48, and 47.62 days respectively. These results suggest that the environmental conditions affecting mortality rates differ, potentially indicative of other ecological factors influencing mosquito populations in each region. Understanding these dynamics is crucial for informing public health strategies related to mosquito control and dengue transmission risk.

4.4 Mosquito biting rate

Mosquito feed human blood for the purpose of meal. Due to this, it search for human to bite them. However, the rate of biting depend on temperature[20, 17]. So that, the biting rate of mosquito is give as

$$b(T) = k(T^2 - T_{min}T)(\sqrt{T_{max} - T}). \tag{4.8}$$

Where $k = 2.03 \times 10^{-4}$, $T_{min} = 10.25^oC, T_{max} = 38.32^oC$ and T is mean temperature.

Implementing the biting rate given in (4.8) with the area under the study we get:

First, we find the mean temperature of the high transmission months in each region.

$$\text{Mean}T_{Dire\ Dawa} = \frac{28+29+29+28+27}{5} = 28.2\,^\circ C$$

$$\text{Mean}T_{Afar} = \frac{26+27+29+31+30}{5} = 28.6\,^\circ C$$

$$\text{Mean}T_{Somali} = \frac{29+28+27+26}{4} = 27.5\,^\circ C$$

Now, let's calculate the biting rate for each region using the mean temperatures.

Computing biting rate for Dire Dawa we get:

$$\begin{aligned} b(28.2) =& 2.03 \times 10^{-4} \left((28.2^2 - 10.25 \cdot 28.2)\sqrt{(38.32 - 28.2)}\right) \\ \approx& 3.269 \times 10^{-1} \text{ (or approximately 0.3269 per day).} \end{aligned}$$

Following the same processes for Afar:

$$\begin{aligned} b(28.6) =& 2.03 \times 10^{-4} \left((28.6^2 - 10.25 \cdot 28.6)\sqrt{(38.32 - 28.6)}\right) \\ b(28.6) =& 3.389 \times 10^{-1} \approx 0.3389 \,\text{per day.} \end{aligned}$$

Similarly, for Somali:

$$\begin{aligned} b(27.5) =& 2.03 \times 10^{-4} \left((27.5^2 - 10.25 \cdot 27.5)\sqrt{(38.32 - 27.5)}\right) \\ b(27.5) =& 3.168 \times 10^{-1} \approx 0.3168 \text{per day.} \end{aligned}$$

Hence, based on the mean temperatures of high transmission risk months we observe that:

Afar has the highest biting rate at approximately 0.3389. Dire Dawa follows with 0.3269. Somali has the lowest biting rate at approximately 0.3168. This analysis suggests that even though all regions have significant vulnerability, Afar appears to have the highest potential for dengue transmission based on biting rates during peak months.

4.5 Bi-transmission Probabilities

According to [23], the transmission probabilities from mosquito to human and vice versa are given as follows:

$$\alpha(T) = 0.001044T(T - 12.286)\sqrt{32.461 - T},\ (12.286 < T < 32.461)^oC. \tag{4.9}$$

Plugging the mean temperature of the areas under consideration we get,

$$\alpha(T)_{Dire\ Dawa} = 0.967,\ \alpha(T)_{Afar} = 0.957,\ \alpha(T)_{Somali} = 0.972.$$

$$\beta(T) = \begin{cases} 0.729T - 0.9037,\ (12.4 \le T \le 26.1)^oC \\ 1,\ (26.1 < T < 32.5)^oC \end{cases}$$

Here, since temperature range in $(26.1 < T < 32.5)^oC$,

$$\beta(T)_{Dire\ Dawa} = \beta(T)_{Afar} = \beta(T)_{Somali} = 1.$$

Here this results are only for selective months particularly, June–August as yearly optimal temperature in these regions.

4.6 Progression rate

The rate at which vulnerable adult female mosquito move into infected class due to a pathogen transmitted from infected human which consists Extrinsic Incubation Period(EIP). EIP is the time taken to the dengue virus inside mosquito before it can be transmitted, that can determined by external factors such as climate change, particularly temperature.

$$\begin{aligned} EIP(T) =& e^{5.2-0.123T} \text{ Where T is optimal temperature of a given region} \\ \rho(T) =& \frac{1}{EIP} = e^{-(5.2-0.123T)}. \end{aligned} \tag{4.10}$$

We need to evaluate $\rho(T)$ at the mean temperatures previously calculated for the high-risk months of each region under equation (4.8).

Mean Temperatures from Previous Analysis

$$\text{Dire Dawa: } T = 28.2°C, \text{ Afar: } T = 28.6°C, \text{ Somali: } T = 27.5°C$$

Using the mean temperatures, we will compute the extrinsic incubation period $EIP(T)$ for each region:

$$\begin{aligned} \text{Dire Dawa: } EIP(28.2) =& e^{5.2-0.123\times 28.2} \approx 5.65 \text{ days.} \\ \text{Afar: } EIP(28.6) =& e^{5.2-0.123\times 28.6} \approx 5.378 \text{ days.} \\ \text{Somali: } EIP(27.5) =& e^{5.2-0.123\times 27.5} \approx 6.16 \text{ days.} \end{aligned}$$

Its physical meaning is for example in Dire Dawa, EIP(28.2) = 5.65 days implies that, after a mosquito bites an infected human and becomes exposed, it takes 5.65 days for dengue virus to develop inside it before it can infect another human.

$$\begin{aligned} \rho(28.2)_{Dire\ Dawa} =& \frac{1}{EIP_{Dire\ Dawa}} \approx 0.177 \text{ per a day.} \\ \rho(28.6)_{Afar} =& \frac{1}{EIP_{Afar}} \approx 0.186 \text{ per a day.} \\ \rho(27.5)_{Somali} =& \frac{1}{EIP_{Somali}} \approx 0.162 \text{ per a day.} \end{aligned}$$

Based on the calculations of the progression rates, the region with the highest incubation completion is Afar with approximately 0.186 while Dire Dawa follows with 0.177, and Somali has the lowest such transition rate at 0.162. A value of 0.186 would mean that, on average, an exposed Aedes mosquito will become infectious after approximately 5.378 days, which has similar meaning for the rest one.

Thus, Afar is the region with the shortest EIP which occur at optimal temperature according to the given formula and mean temperature assessments.

Human death rate

To compute human death rate, we used the average life span (LE) of Dire Dawa, Afar, and Somali regions which is 67 years.

$$\mu_h = \frac{1}{LE} = \frac{1}{67 \times 365.25} = 0.00004 \text{ per a day.}$$

Human birth rate

$$\Lambda_h = \mu_h \times N_h = 0.00004 \times 8,445,050 = 345 \text{ person per day.}$$

,N_h be total populations of Dire Dawa, Afar, and Somali region.

4.7 Seasonal Transmission rate

Dengue transmission exhibits seasonal variation driven by the cyclical interplay between mosquito and human populations. In this study, transmission rate is split into biting rate and transmission probabilities. Collectively, the transmission rate from mosquito to human, α', is modulated by a cosine function with a period of one year, peaking during warmer months. This is represented as $\alpha' = \alpha_0(1 + \omega_1 \cos(\frac{2\pi(t-\Phi)}{365}))$, where $\alpha_0 = 0.25$ is the baseline transmission rate, $\omega_1 = 0.3$ is the amplitude of seasonal variation (in tropical and subtropical region), and t is time in days. Similarly, human-to-mosquito transmission, β', also varies seasonally, with $\beta' = \beta_0(1 + \omega_2 \cos(\frac{2\pi(t-\Phi)}{365}))$, indicating that transmission from infected humans to mosquitoes is also higher during warmer months, with $\beta_0 = 0.29$ and $\omega_2 = 0.3$ representing the baseline and amplitude of seasonal variation. We employed the value of α_0 and β_0 from fitting whereas ω_1 and ω_2 from [30]. But the phase shift (Φ) indicates the season where the disease become peak. For instance in Ethiopia, the peak season of dengue is August or September (day 220 to 260) in average 240 and the observed data also shows August. Hence, $\Phi = 240$. The detailed impact of this seasonal change is elaborated graphically under section (6).

Symbol	Values	Source
π_1	40.55 Joule	[21]
π_2	0.01	[21]
d	0.000027	Fitted
K	1000/day	[5, 24]
r	(0.02-0.04)C^o	[5, 24]
T_0	$15C^o$	[5, 24]
α	0.78	Fitted
π_e	200	[19]
β	0.91	Fitted
η	(0.01-1)metric-tone	[5, 24]
γ	0.02metric-tone	[5, 24]
δ	0.145 per a day	Fitted
R_f	50-100 mm	[25]
S_p	Eq.4.5	est.
S_{lmax}	0.75	[9]
S_{pmax}	0.55	[9]
τ_e and τ_p	each 1day	[21]
$\theta(T, R_a)$	0.109 per a day	mean(est. + Fitted)
ϕ	0.0149 per a day	Fitted
G_h	(0.1-10)metric-tone	[5, 24]
G_n	(0.1-5)metric-tone	[5, 24]
b_n	(0.01-0.5)/day	[5, 24]
b_d	(0.01-0.04)/day	[5, 24]
$b(T)$	0.321 per a day	mean(est. + Fitted)
Λ_h	Eq. 4.6	est.
$\rho(T)$	0.175 per a day	mean(est. + Fitted)
μ_h	Eq. 4.6	est.
$\mu_m(T)$	0.023 per a day	mean(est. + Fitted)
C_0	2.5metric-tone	[5, 24]
R_a	25mm	[5, 24]

Table 2: Model parameters and their values

Where π_1 stands for Entropy contribution to hatch whereas π_2 represent temperature influence factor to hatch. For a detailed description of the parameters, please see Section (2).

5 Model Validation

To validate the model described in equation (2.1), we conducted a comprehensive analysis utilizing various tools, including model fitting techniques and additional statistical metrics. This approach allows us to assess the model's

performance and reliability, ensuring that it accurately represents the underlying data and fulfills the research objectives. To analyze these tools, monthly collected two years of current dengue case data from the Ethiopian Public Health Institute (EPHI) [7].

Based on the reported cases available in Supplementary materials, the model was fitted to the data as follows. Before using the raw data, the data were scaled to reflect cases per 1,000 people for the simulation.

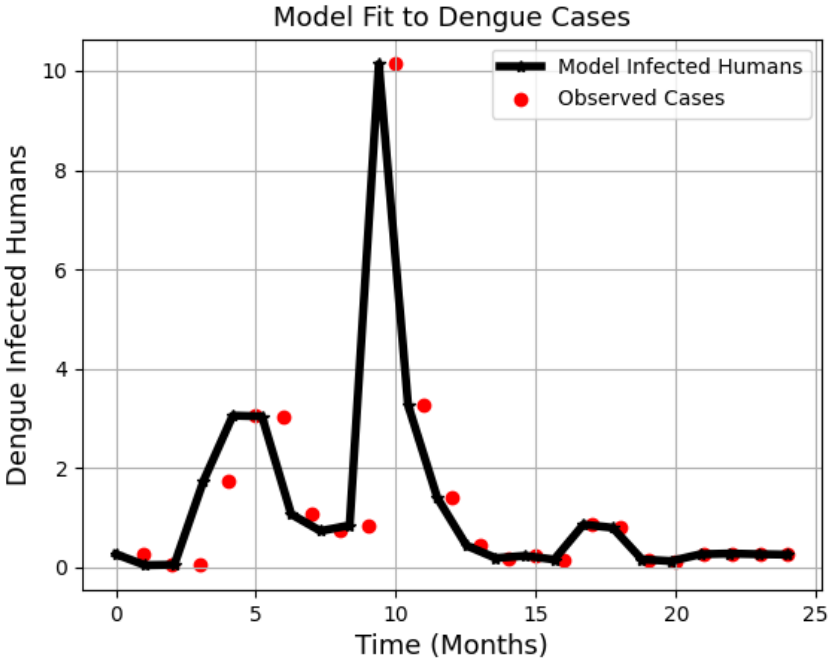

Figure 3: The model fitted to the existing dengue data

Figure 3 shows that, the model that fitted to the prevalence of dengue cases and the y-axis represented number of infected human scaled down by 1,000 people. For instance, $I_h = 10$ on vertical axis stands 10,000 infected people. The graph demonstrates a strong alignment between the model's predictions and actual dengue cases over two years, highlighting a notable peak around the 10th month. The close correspondence during this surge indicates the model effectively captures seasonal or outbreak-driven fluctuations in infection rates. This pattern underscores the importance of targeted interventions during peak periods to mitigate transmission and highlights the model's utility in forecasting and managing dengue outbreaks.

5.1 Statistical Analysis

Based on the fitted model applied to observed cases using Python programming software with RK4 method, we discuss the implications of the fitted parameters, RSSE (Residual Sum of Squares Error), R-squared, AIC (Akaike Information Criterion), confidence intervals, and p-values.

Fitted Parameters: The fitted parameters represent the estimated values of the model parameters after optimization by making climate variable constant. However, climate based parameters were computed lonely for each region under consideration. The results are approximately, similar. These include: $\alpha : 0.7809$, $\beta : 0.9103$, $b : 0.3206$, $\delta : 0.1450$, $\rho : 0.1750$, $\theta : 0.5760$, $\phi : 0.0149$, $d : 0.000027$ (dengue induced death rate), $\mu_m : 0.0220$ (mosquito death rate), and scaling factor: 0.2104.

This implies that the parameters influencing the disease reproduction rate (α and β) are relatively high, suggesting that transmission may be slightly spread within the population. However, the high value of biting rate ensures as many works are expected from public health sector. The parameters δ and ρ provide insights into the progression rates from exposed to infectious stages in humans and mosquitoes, respectively. Additionally, the ϕ parameter indicates the recovery rate for humans. The low death rates for both humans (d) and mosquitoes (μ_m) suggest that the mosquito population and human infections are relatively stable and not particularly lethal.

The residual sum of squares error (RSSE) value is 0.000135, which indicates that the model predictions are closely aligned with the observed data, suggesting a good model fit. On the other hand, the obtained R^2 value is 0.9998938, which is close to 1. This implies that the model explains almost all the variability in the observed data. This suggests an excellent fit and indicates that changes in the predictor variables (the model parameters) are well accounted for in predicting the response variable (the observed data).

AIC (Akaike Information Criterion): The AIC is calculated as:

$$AIC = 2n(E_p) + m\ln(\frac{RSSE}{m}) = \text{Value: } -225.8,$$

where E_p is the number of parameters, and m stands for observed datasets. A lower AIC value generally indicates a better model fit when comparing neglected models. The negative value here demonstrates that the model performs exceptionally well in terms of goodness-of-fit.

Most parameter confidence intervals are not wide. But ϕ: [-1.2094, 1.7879]) which suggests the value of ϕ lies exactly between -1.2094 and 1.7879.

The p-values of most parameters are less than 0.05, indicating statistical significance at conventional levels. This suggests that these parameters are critical predictors in the model and should not be retained in any further analyses or refinements. However, the p-value for d : 0.5756 which is greater than 0.05, indicating that its contribution is relatively less significant when considering the model collectively.

Overall, the model appears to fit the data very well, satisfying almost all statistical criteria, thereby ensuring that the model is biologically interpretable and useful in real-world applications.

6 Numerical Simulation

To perform numerical simulation, we employed Python programming language software to visualize the stated objective those that mentioned theoretically. To do so, we used values of parameters which stated in Table 2. The detail results of graphical representations with its theoretical descriptions were discussed as follow.

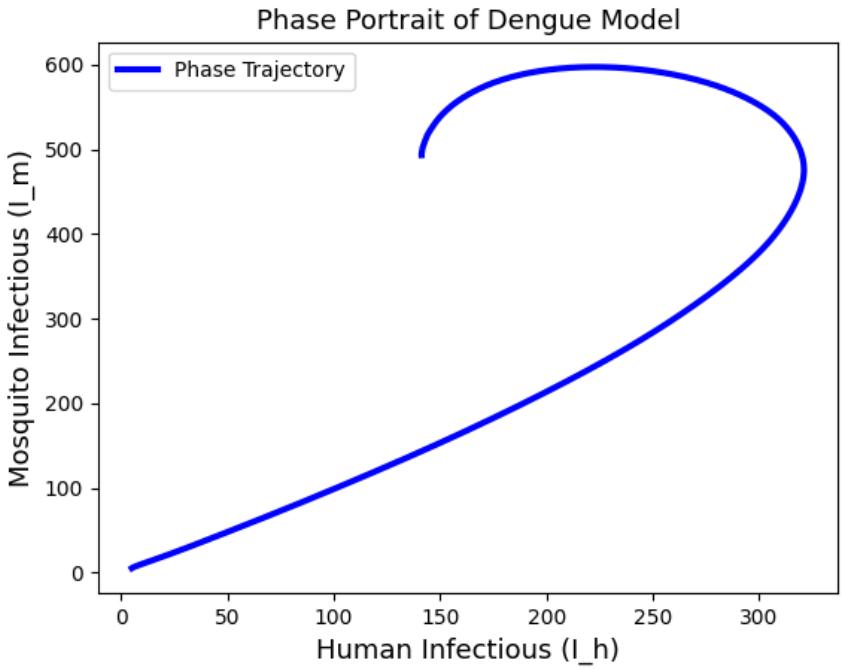

Figure 4: The global solution of infected class of the model

The phase portrait of the dengue model of Figure 4 shows the dynamic relationship between infected humans and mosquitoes over time. Initially, as human infections increase, mosquito infections also rise, illustrating the transmission

cycle. The looping pattern indicates oscillations or cyclical behavior, possibly due to seasonal factors, highlighting the interconnected and cyclical nature of dengue spread between humans and mosquitoes.

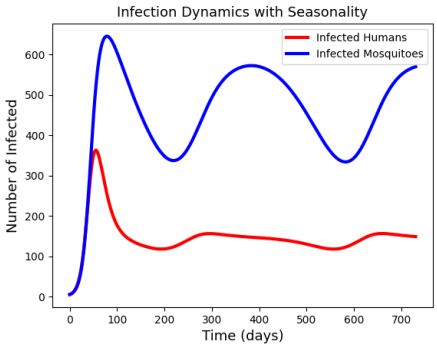

(a) Impact of Seasonal variation on infected human and mosquito

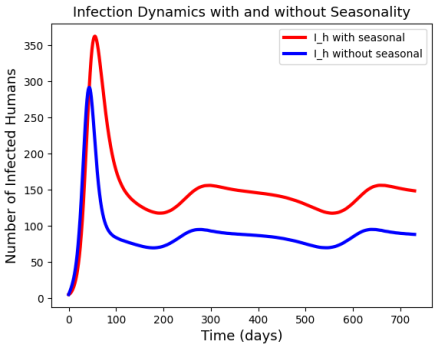

(b) Transmission rate with and without seasonal change

Figure 5: Impact Seasonal variation on Transmission rate of dengue disease

Figure 5a and 5b show the application of seasonal change to the model, amplifying infected mosquitoes followed by infected humans, and how fluctuations in season potentially affect the dengue transmission rate, respectively.

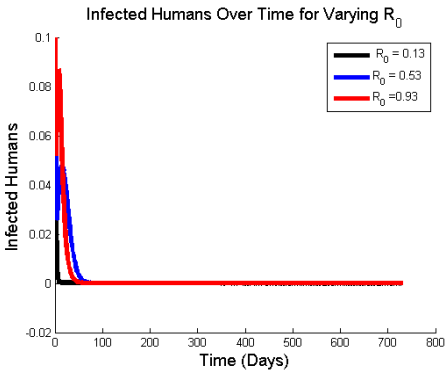

(a) Global stability of infected human at DFE for different $R_0 < 1$

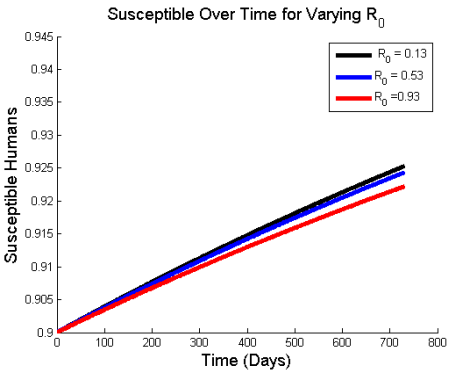

(b) Global stability of susceptible human at DFE for varying R_0

Figure 6: Illustration of global stability of DFE for different $R_0 < 1$

Figure 6a shows that for $R_0 < 1$, the trajectories of infected individuals with different R_0 values all decay to zero over time. Conversely, the number of susceptible individuals increases with time, as revealed in Figure 6b. These observations confirm that E_0 is globally stable.

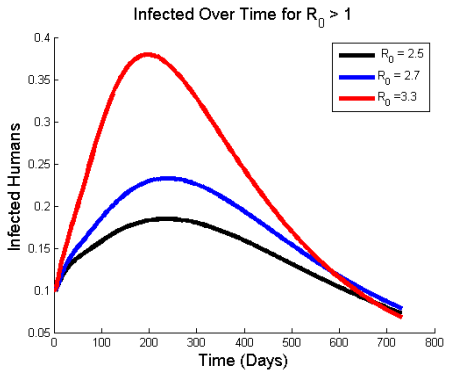

(a) Global stability of infected human at EE for different $R_0 > 1$

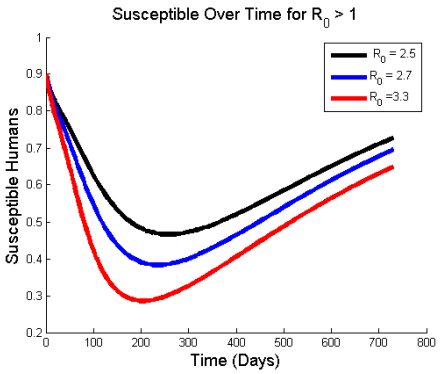

(b) Global stability of susceptible human at EE for different R_0

Figure 7: Demonstration of global stability of EE for different $R_0 > 1$

Figure 7a illustrates that for $R_0 > 1$, the trajectories of infected individuals with different R_0 values all tend to some point (EE) as time increases. Conversely, the number of susceptible individuals decreases substantially due to the presence of infection, as shown in Figure 7b. Ultimately, all trajectories converge to a positive constant(EE). This implies that EE is globally stable.

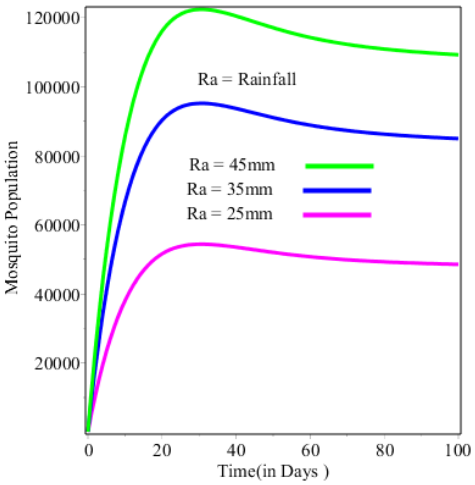

(a) Impacts of rainfall on mosquito population

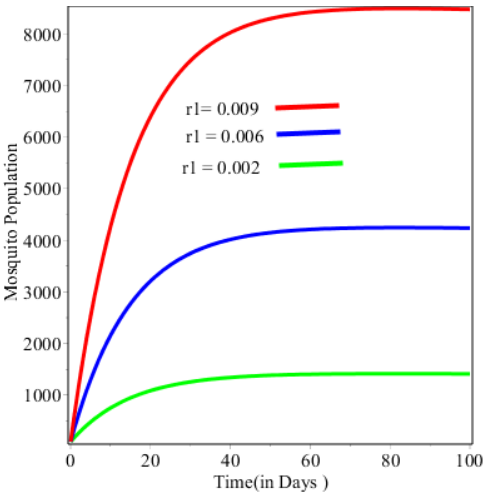

(b) Effects of growth rate of carbon-dioxide concentration on mosquito population

Figure 8: Impact of climate change on mosquito population dynamics

Figure 8a shows that, rainfall is potentially contribute in increasing mosquito population. However, heavy rainfall can flush out the immature stage of mosquito population. On other hand, as the growth rate of temperature due to the growth of carbon-dioxide from human activities increase, the mosquito population highly increase which is clearly revealed in Figure 8b.

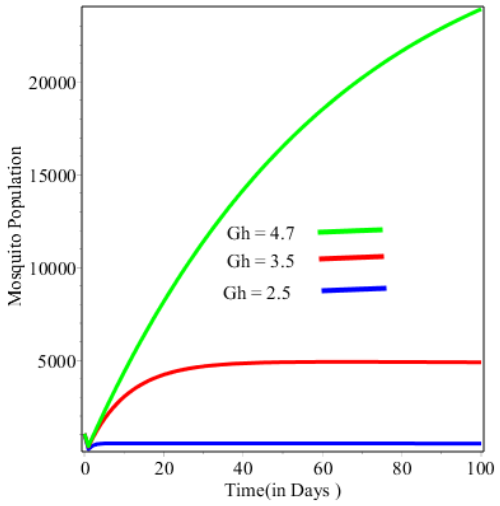

(a) Impacts temperature due to human activities on mosquito population

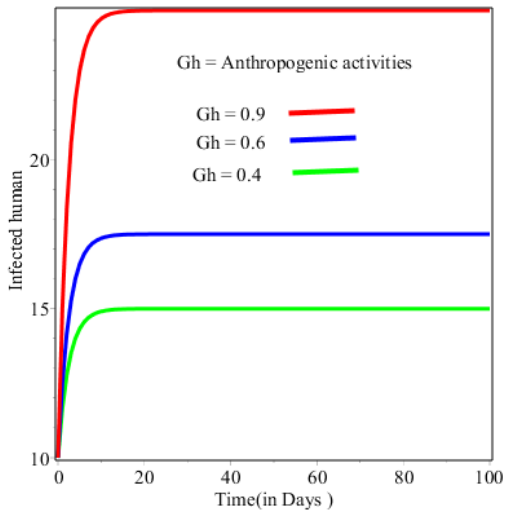

(b) Effects of growth rate of carbon-dioxide concentration on infected human

Figure 9: Impact of climate change on mosquito population and infected human

Figure 9a shows, as the rate of anthropogenic activities increase, the mosquito dynamics increase. Similarly, Figure 9b indicates, as the rate of anthropogenic activities increase, infected human slightly step up.

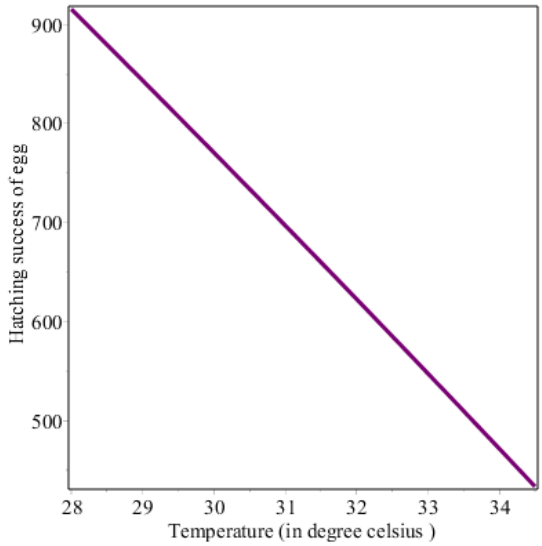

(a) Impacts of temperature on hatching success of eggs

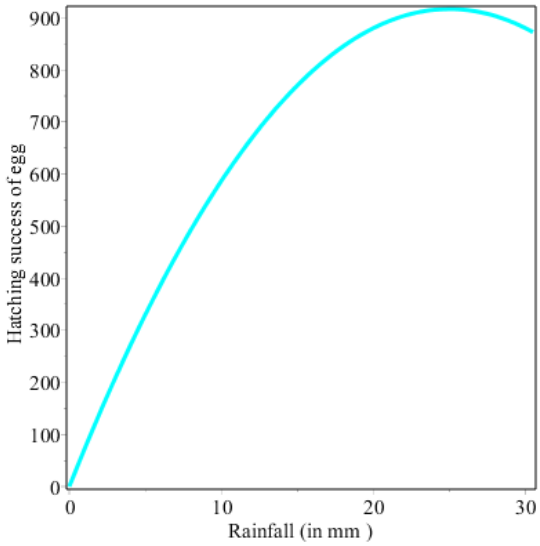

(b) Effects of rainfall on hatching success of eggs

Figure 10: Impact of climate change on hatching success of eggs, larvae and pupae

The hatching success of eggs of mosquito potentially depend on both temperature and rainfall, which is depicted in Figure 10a and 10b respectively.

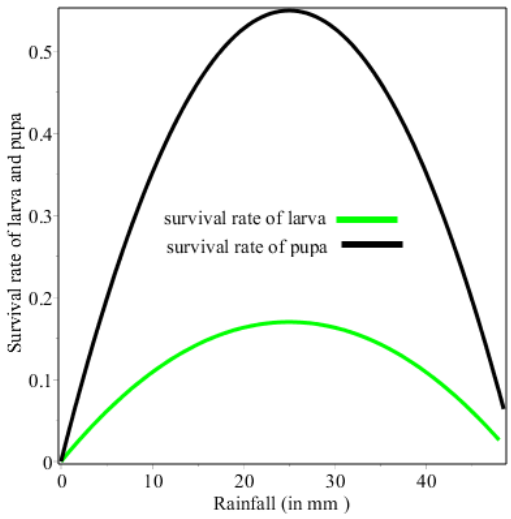

(a) Effects of rainfall on survival rate of larva and pupa

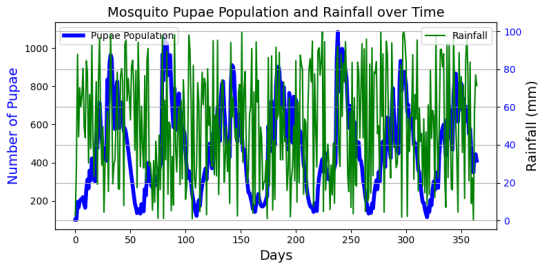

(b) Simulation of rainfall fluctuation via pupae

Figure 11: Effect of Rainfall on larvae and pupae

As shown in Fig.11a, rainfall determine the growth rate of both larvae and pupae. In line to this, Fig.11b illustrate the intensity of rainfall in relation to pupae.

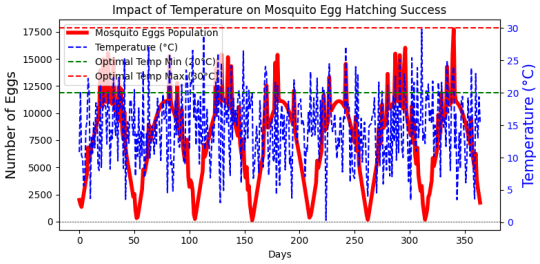

(a) Simulation of temperature variation via mosquito's eggs

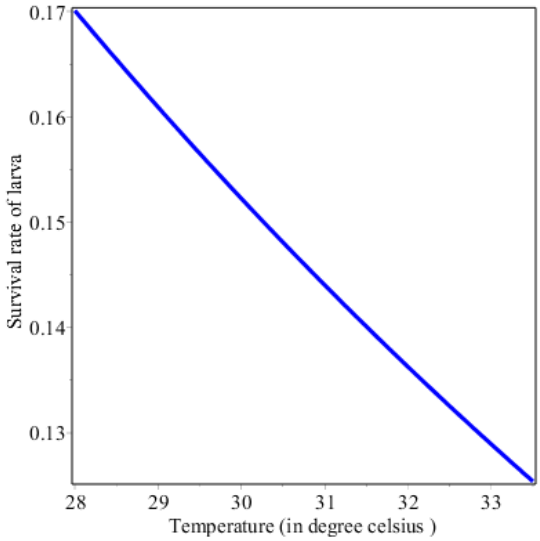

(b) Impact of temperature on the survival rate of larva

Figure 12: Impact of climate variation on the survival rate of Aedes aegypti's larva

Figure 12a vividly illustrates the profound impact of temperature on mosquito eggs, highlighting how changes in temperature can significantly influence their development. Conversely, Figure 12b clearly demonstrates that the larval survival rate sharply declines as temperatures rise, underscoring the sensitive relationship between temperature and larval viability.

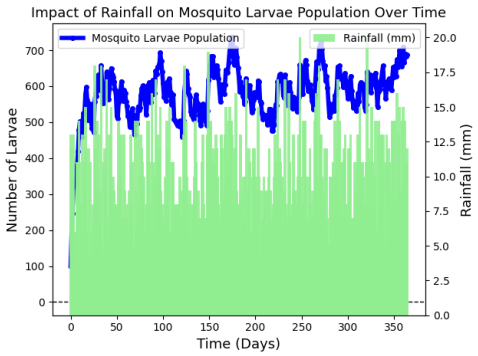

(a) Simulation of Rainfall via Mosquito's Larvae

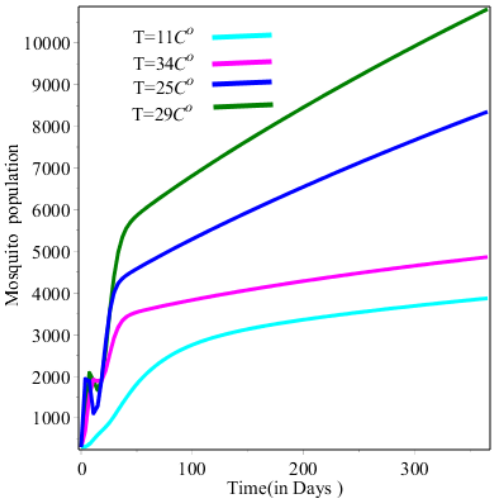

(b) Impact of temperature on mosquito population

Figure 13: Impact of climate change on survival rate of Eggs and Larvae

The growth rate of pupae can be sustained during low and medium rainfall, as shown in Figure 13a. This suggests that, while higher temperatures improve hatching success, rainfall also plays a role in promoting the development of larvae into pupae. On the other hand, Figure 13b shows that optimal temperatures increase the size of the mosquito population, but at low and high temperatures, the population decreases.

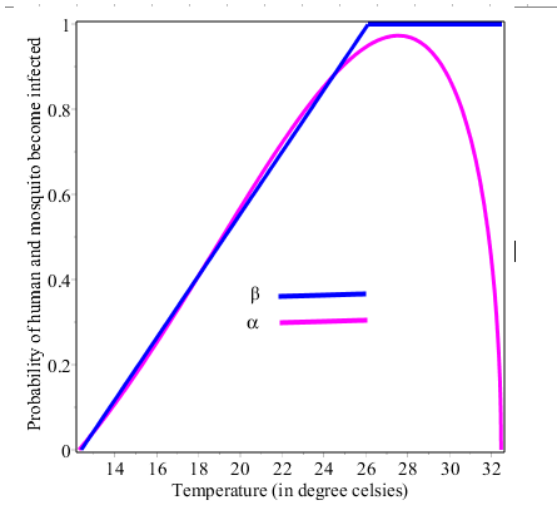

(a) The relationship between probability of dengue transmission and temperature

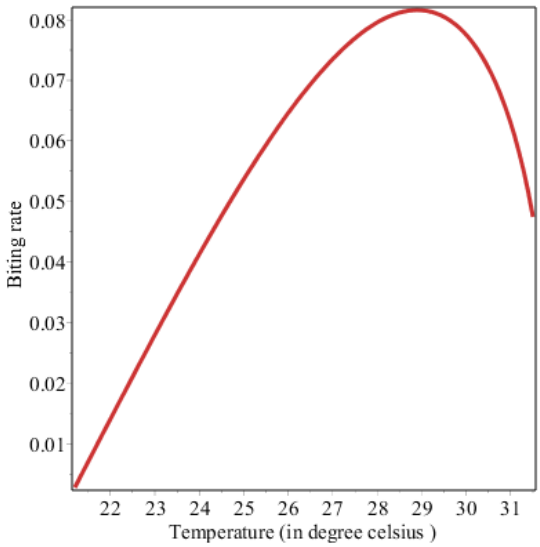

(b) Biting rate of adult mosquito via temperature

Figure 14: Impact of temperature on dengue transmission probabilities and the rate mosquito biting.

Figure 14a shows that, the impact of temperature on the probability that a bitten individual become infected and conversely the mosquito itself gets infectious. On other hand, Figure 14b shows that, as temperature that ranged in $(21-30)C^o$ increase, the biting rate of mosquito ascended.

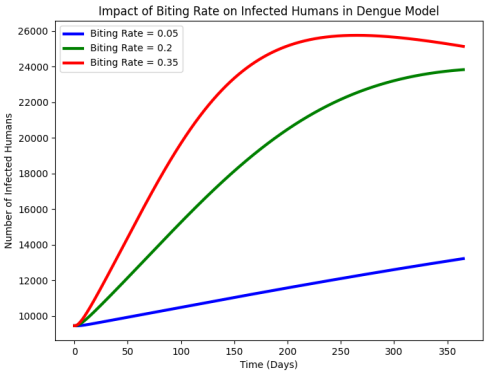

(a) The relationship between the rate of bite and infection progress

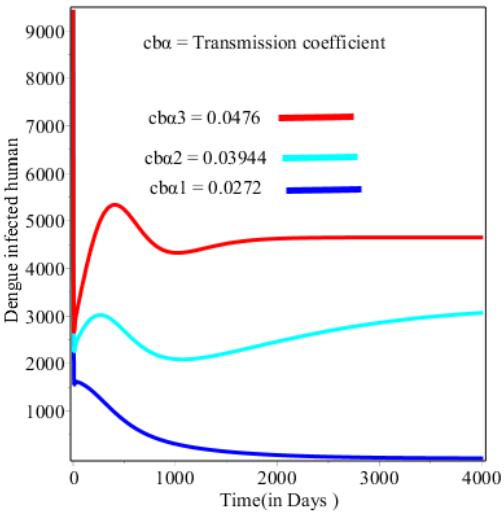

(b) Impact of interaction of mosquito and human

Figure 15: Impact of climate change on biting rate of adult mosquito and dengue outbreak

Figure 15a suggests that mosquito biting significantly intensifies the number of infected humans. As the biting rate increases, even slightly, the number of infectious individuals rapidly rises, accelerating the disease outbreak. Consequently, this contributes to the spread of the disease, as evident in Figure 15b. This figure illustrates an increase in the number of dengue-exposed individuals due to the presence of a high magnitude of infected mosquito bites. As a result, the number of infected individuals continues to rise over time. Furthermore, it shows the prevalence of the disease in the absence of any intervention measures.

7 Results and Discussion

This section explores the relationship between climate change and mosquito populations, emphasizing its influence on dengue transmission dynamics. We employed an extended deterministic model $S_hE_hI_hR_h - S_mE_mI_m$ with climate-sensitive entomological parameters, demonstrating that dengue transmission is highly responsive to weather variations particularly temperature and rainfall. Our analysis indicates that human activities, alongside natural events, contribute to rising temperatures, which in turn facilitate mosquito reproduction. Activities such as deforestation, industrial expansion, and increased transportation release carbon dioxide, leading to temperature increases that affect pathogen development and mosquito life cycles.

Model results show that the disease-free equilibrium is locally asymptotically stable when $R_0 < 1$, especially if interactions between mosquito and human populations are well-managed; otherwise, this equilibrium remains unstable. Additionally, we identified the existence of a unique positive equilibrium, indicating the potential for sustained dengue presence within a community. Sensitivity analysis revealed key parameters such as the probability of transmission to a host (α), the probability of a mosquito becoming infectious after biting an infected individual (β), and the pupa survival rate (θ) which significantly accelerate outbreaks and account for approximately 50% of the increase in cases. Notably, the biting rate (b) emerged as the most sensitive parameter influencing disease transmission, underscoring its critical role. Conversely, parameters like d, and ϕ showed lower sensitivity.

To validate these findings, we conducted numerical simulations focusing on three regions in Ethiopia: Afar, Dire Dawa, and Somali identified as high-risk areas for dengue. Using reported monthly case data from early 2023 to the end of 2024, we fitted the model, with the results shown in Figure 3, demonstrating a strong correlation between observed cases and model predictions.

The phase portrait in Figure 4 illustrates how the numbers of infected humans and mosquitoes evolve over time. Initially, as human infections rise, mosquito infections follow, creating a cyclical pattern. This suggests a recurring transmission cycle, possibly influenced by seasonal factors. Overall, the model underscores the interconnectedness of human and mosquito populations and the potential for ongoing disease cycles.

Figures 5a and 5b depict how seasonal variations can lead to an initial increase in infected mosquitoes, followed by a rise in infected humans, highlighting the seasonal impact on dengue spread. Figure 6a shows that when $R_0 < 1$,

the number of infected individuals declines to zero over time, while susceptible individuals increase confirming the stability of the disease-free equilibrium. Conversely, Figure 7a demonstrates that when $R_0 > 1$, infected cases stabilize at a positive level, and susceptible numbers decrease, indicating the establishment of a stable endemic equilibrium.

Our analysis of climate-dependent entomological parameters reveals that egg hatching success and larval survival are significantly affected by temperature and rainfall, as shown in Figures 10a, 10b, and 12b. Hatching success and larval survival decline at extremely high temperatures, with an optimal temperature of approximately 28°C for maximum egg hatching. Figure 13b highlights a sharp increase in mosquito populations at around 30°C, followed by declines at higher and lower temperatures. Similarly, Figures 11a and related data indicate that larval and pupa survival are highly sensitive to rainfall, with survival rates dropping sharply above 50 mm corroborating previous studies [21, 23].

Moderate rainfall appears conducive to pupal survival, whereas excessive rainfall disrupts their development, as shown in Figures 10b and 11a. Climate change may lead to larger populations of female Aedes mosquitoes that feed on humans, aligning with findings from [17]. Figure 14a illustrates how temperature influences the likelihood of infection in bitten individuals and the probability of mosquitoes becoming infectious, with pathogen development and transmission rates being temperature-dependent. Furthermore, Figure 14b indicates that biting rates increase with temperatures between 21°C and 30°C, contributing to higher mosquito densities and increased feeding activity among adult females.

The model also emphasizes that human activities such as deforestation and industrialization amplify carbon dioxide levels, promoting mosquito proliferation and increasing human infections, consistent with [5]. Simulation results in Figure 15a reinforce that higher mosquito biting rates, driven by temperature, correlate with increased cases, underscoring the endemic potential of dengue.

Table 1 presents parameter values such as H_s, S_p, S_l, and θ for the three regions. Dire Dawa exhibits the highest values ($H_s = 0.607$, $S_p = 0.329$, $S_l = 0.0334$, $\theta = 0.151$), indicating more favorable conditions for mosquito development, while Afar shows lower values ($H_s = 0.0877$, $S_p = 0.473$, $S_l = 0.04702$, $\theta = 0.045$). Somali's parameters fall in between, suggesting regional environmental differences influence mosquito dynamics.

Analysis of mosquito mortality rates indicates Afar has the highest death rate (0.023/day), followed by Dire Dawa (0.022/day), with Somali the lowest (0.021/day). Correspondingly, the average lifespan of mosquitoes ranges from approximately 43.5 to 47.6 days across regions. Afar's higher biting rate (0.339) and shorter extrinsic incubation period (5.38 days) suggest a higher transmission potential, consistent with [16] findings that increased temperatures accelerate viral development within mosquitoes.

Regional variations in transmission probabilities $\alpha(T)$ being 0.967 in Dire Dawa, 0.957 in Afar, and 0.972 in Somali along with the stable transmission probability from mosquitoes to humans within 26.1°C to 32.5°C, highlight the influence of temperature on infection dynamics.

In general, temperature and rainfall are critical factors in shaping the behavior of *Aedes* mosquitoes and the transmission of dengue, especially in tropical regions. The model emphasizes that rainfall levels between 30 mm and 40 mm support increased pupal survival and adult mosquito populations, thereby elevating transmission risk.

8 Conclusion

This study provides a comprehensive analysis of the relationship between climate change and dengue transmission dynamics, specifically through the lens of mosquito populations. By employing an extended deterministic model, we demonstrated that fluctuations in temperature and rainfall have a profound impact on dengue transmission and mosquito reproduction. Human activities, notably deforestation, industrial growth, and increased transportation, exacerbate climate change by raising temperatures, which, in turn, facilitate both the reproduction of mosquitoes and the development of pathogens responsible for dengue. Key findings from our analysis indicate that the disease-free equilibrium becomes locally asymptotically stable when the basic reproduction number R_0 is less than one, highlighting the importance of managing interactions between mosquito and human populations to prevent outbreaks. Conversely, the existence of a unique positive equilibrium emphasizes the persistent risk of dengue within communities. Through sensitivity analysis, we identified critical parameters namely the transmission probability of infection α, the infection probability post-bite β, and the pupa survival rate θ which significantly contribute to the surge in dengue cases, accounting for 50% of the observed increases. Furthermore, biting rates emerged as pivotal factor in disease transmission, accentuating their roles in outbreak dynamics. In our numerical simulations spanning at-risk regions of Afar, Dire Dawa, and Somali, we validated the model against real data, revealing a strong alignment between reported cases and predictions. The findings underscore that climate-sensitive parameters substantially influence mosquito

life cycles, with optimal conditions at around $28°C$ for egg hatching and variable impacts of rainfall on both pupae survival and mosquito populations. Particularly concerning is the Somali region, which exhibits the highest metrics for mosquito survival ($\theta = 0.733$), biting rates (0.163), and infectious rates (approximately 9.910 infections per mosquito per month). These metrics indicate a particularly heightened potential for dengue transmission compared to Afar and Dire Dawa. Human and natural activities are also significant contributors to climate change, which, in turn, play a crucial role in the spread of mosquito-borne diseases such as dengue fever. However, in this study, our focus is limited to the impact of temperature and rainfall, two climate variables that are particularly relevant to the spread of dengue virus. Overall, our research highlights the intricate interplay between climate factors and mosquito-borne diseases like dengue, emphasizing the urgent need for targeted public health interventions in vulnerable regions. Understanding these dynamics is crucial for developing effective strategies for mosquito control and disease prevention, as rising temperatures and altered rainfall patterns may significantly shift dengue transmission dynamics in the future.

Acknowledgment

First and foremost I would like to thank, almighty God who often with me. Secondly, I would like to express my special appreciation to all of my reviewers and families who helps me both ideally and morally, specially Dr. Solomon Girma and my son Omega Abraham for their continuous guidance and support.

Author Contributions

The initial draft, conceptualization, visualization, and editing were done by A.G, while G.T and B.T provided positive reviews for each section. All authors have also read and approved the final version of the manuscript.

Funding

This research received no external funding.

Data Availability

The data used in this work are available from the corresponding author upon request and the resources are properly cited.

Conflicts of Interest

The authors declare that, there are no conflicts of interest on this work.

References

[1] L.J.S. Allen, *An Introduction to Mathematical Biology*, Pearson, 2008.

[2] A.R. Barr, *Growth and development of Aedes aegypti (L.) (Diptera: Culicidae) in relation to temperature*, Bull. Entomol. Res. **71** (1981), no. 4, 531–538.

[3] O.J. Brady and S.I. Hay, *The first global model of Zika virus transmission*, Sci. Rep. **3** (2013), 3296.

[4] F. Brauer, C. Castillo-Chavez, and Z. Feng, *Mathematical Models in Epidemiology*, Springer, 2019.

[5] G. Chowell, K. Mizumoto, J.M. Banda, S. Poccia, and C. Perrings, *Assessing the potential impact of vector-borne disease transmission following heavy rainfall events: a mathematical framework*, Philos. Trans. R. Soc. B **374** (2019), 20180272.

[6] Ethiopian Meteorological Institute (EMI), *Historical climate reports for Afar, Dire Dawa, and Somali regions*, 2025.

[7] Ethiopia Public Health Institution (EPHI), 2025.

[8] L. Esteva and C. Vargas, *Analysis of a dengue disease transmission model*, Math. Biosci. **150** (1998), 131–151.

[9] G. Obholz, G.S. Blas, S. Fischer, and A. Diaz, *Winter survival of Aedes aegypti (Diptera: Culicidae) eggs at its southern limit distribution*, Acta Trop. **231** (2022), 106471.

[10] G. Hertzler, *A stochastic differential equation for modeling the "classical" probability distributions*, in 47th Aust. Agric. Econ. Soc. (AAES) Conf., Fremantle, Australia, pp. 12–14, 2003.

[11] T.H. Jetten and D.A. Focks, *Potential changes in the distribution of dengue transmission under climate warming*, Am. J. Trop. Med. Hyg. **57** (1997), 285–297.

[12] A. Khan, M. Hassan, and M. Imran, *Estimating the basic reproduction number for single-strain dengue fever epidemics*, Infect. Dis. Poverty **1** (2014), 12.

[13] J.E. Kim, Y. Choi, J.S. Kim, S. Lee, and C.H. Lee, *Potential effects of climate change on dengue transmission dynamics in Korea*, PLoS ONE **13** (2020), no. 6, e0199205.

[14] H. Lee, J.E. Kim, S. Lee, and C.H. Lee, *Potential effects of climate change on dengue transmission dynamics in Korea*, PLoS ONE **13** (2018), no. 6, e0199205.

[15] J. Liu-Helmersson, H. Stenlund, A. Wilder-Smith, and J. Rocklov, *Vectorial capacity of Aedes aegypti: effects of temperature and implications for global dengue epidemic potential*, PLoS ONE **9** (2014), no. 3, e89783.

[16] R. Lowe et al., *Deterministic and stochastic models for predicting the effects of climate change on the transmission of dengue fever*, Environ. Res. Lett. **10** (2015), no. 2, 024008.

[17] E.A. Mordecai, J.M. Cohen, M.V. Evans, P. Gudapati, L.R. Johnson, C.A. Lippi, K. Miazgowicz, C.C. Murdock, J.R. Rohr, S.J. Ryan, V. Savage, M.S. Shocket, M. Stewart Ibarra, M.B. Thomas, and D.P. Weikel, *Detecting the impact of temperature on transmission of Zika, dengue, and chikungunya using mechanistic models*, PLoS Negl. Trop. Dis. **11** (2017), e0005568.

[18] M. Otero, H.G. Solari, and N. Schweigmann, *A stochastic population dynamics model for Aedes aegypti: formulation and application to a city with temperate climate*, Bull. Math. Biol. **68** (2006), 1945–1974.

[19] P.E. Parham and E. Michael, *Modelling climate change and malaria transmission*, in Modelling Parasite Transmission and Control, Springer New York, pp. 184–199, 2010.

[20] S. Polwiang, *The seasonal reproduction number of dengue fever: Impacts of climate on transmission*, PeerJ **3** (2015), e1069.

[21] M.M. Rossi, L.F. Lopez, and E. Massad, *The dynamics of temperature- and rainfall-dependent dengue transmission in tropical regions*, Ann. Biom. Biostat. **2** (2015), 1–6.

[22] L. Rueda, K. Patel, R. Axtell, and R. Stinner, *Temperature-dependent development and survival rates of Culex quinquefasciatus and Aedes aegypti (Diptera: Culicidae)*, J. Med. Entomol. **27** (1990), 892–898.

[23] G. Sanchez-Gonzalez and R. Conde, *Mathematical modeling of dengue virus serotypes propagation in Mexico*, PLoS ONE **18** (2023), no. 7, e0288392.

[24] S. Singh, *Modeling the effect of global warming on the spread of carrier dependent infectious diseases*, Model. Earth Syst. Environ. **3** (2017), no. 1, 1–10.

[25] K.H. Thai, S Zhao, Y Wei, K Li, X Jiang, C Li, C. Ren, S. Yin, J. Ho, J. Ran, and L. Han, *Rainfall variability and dengue transmission in Southeast Asia*, Trop. Med. Int. Health **15** (2010), no. 6, 759–768.

[26] Y. Wang, S. Zhao, Y. Wei, K. Li, X. Jiang, C. Li, C. Ren, S. Yin, J. Ho, J. Ran, L. Han, B.C.Y. Zee, and K.C. Chong, *Impact of climate change on dengue fever epidemics in South and Southeast Asian settings: A modeling study*, Infect. Disease Modell. **8** (2023), no. 3, 645–655.

[27] World Health Organization, *Dengue and Dengue Hemorrhagic Fever: Diagnosis, Treatment, Prevention and Control*, 1997.

[28] World Health Organization, *Dengue and severe dengue*, 2022.

[29] World Health Organization (WHO), *Guidelines for Testing Mosquito Adulticides for Indoor Residual Spraying and Space Spray*, WHO, Geneva, 2013.

[30] *Modeling seasonal variation of dengue transmission in Thailand*.